A family of readily synthesised phosphorescent platinum(II) complexes based on tridentate *N^N^O*-coordinating Schiff-base ligands

Emma V. Puttock, Jack D. Fradgley, Dmitry S. Yufit and J. A. Gareth Williams *

Department of Chemistry, Durham University, Durham, DH1 3LE, U.K.

** E-mail: j.a.g.williams@durham.ac.uk*

Abstract

The synthesis and photophysical properties of 22 platinum(II) complexes featuring *N^N^O*-coordinating ligands are described. The complexes have the form Pt(*N^N^O*-L^n)Cl (n = 1 to 20). The tridentate ligands comprise of lateral pyridine and phenolate rings, offering the metal N and O coordination respectively, linked via an imine or hydrazone unit that provides a further, central N atom for coordination. The proligands HL^n, some of which have previously been reported for the coordination of 1st row transition metal ions in other contexts, are Schiff bases that are readily synthesised by condensation of salicylaldehydes either with 8-aminoquinoline (to generate imine-based ligands HL$^{1–4}$) or with 2-hydrazinopyridines (to generate hydrazone-based proligands HL$^{5–20}$). The Pt(II) complexes are prepared under mild conditions upon treatment of the proligands with simple Pt(II) salts. Metathesis of the chloride ligand by an acetylide is possible, as exemplified by the preparation of two further complexes of the form Pt(*N^N^O*-L^n)(-C≡C-Ar), where Ar = 3,5-bis(trifluoromethyl)phenyl. Nine of the complexes have been characterised in the solid state by X-ray diffraction. The imine-based complexes have intense low-energy absorption bands around 520 nm attributed to charge-transfer transitions. They display deep red phosphorescence in solution at ambient temperature, with λ_{max} in the range 635 – 735 nm, quantum yields up to 4.6% and lifetimes in the microsecond range. The hydrazone complexes that feature a py–NH–N=C–Ar linker display pH-dependent absorption spectra owing to the acidity of the hydrazone NH: these complexes have poor photostability in solution. In contrast, their N-methylated analogues (*i.e.*, py–NMe–N=C–Ar) show no evidence of photodecomposition. They are phosphorescent in solution at room temperature in the 600–640 nm region, the emission maximum being influenced by substituents in the phenolate ring. The results show how simply prepared tridentate Schiff base ligands – which offer the metal a combination of 5- and 6-membered chelate rings – can provide access to phosphorescent Pt(II) complexes that have superior emissive properties to those of terpyridines, for example.

INTRODUCTION

There has been extensive interest in the photophysical and photochemical properties of platinum(II) complexes over recent years.[1] Much of the recent research has been driven by applications that exploit phosphorescence from such complexes, such as triplet phosphors for organic light-emitting diodes (OLEDS);[2] probes and labels for biological imaging,[3] including time-resolved emission microscopy;[4] and optical sensors for molecular oxygen that rely on quenching of long-lived excited states.[5] In parallel, other applications are based on the use of the triplet excited-states in sensitizing processes such as triplet-triplet annihilation upconversion[6] and singlet oxygen generation for potential phototherapeutic applications.[7] Owing to the high spin-orbit coupling (SOC) constant of platinum, intersystem crossing in low-molecular-weight Pt(II) complexes is typically much faster than fluorescence, and the triplet state T_1 is populated with high efficiency. Efficient SOC pathways also promote the subsequent, formally forbidden $T_1 \rightarrow S_0$ phosphorescence process.[8]

In addition to a high radiative rate constant, high quantum yields are typically favoured by a high degree of rigidity to disfavour non-radiative decay processes that involve structural distortion in the excited state.[9] In this respect, tridentate ligands might be anticipated to be superior to related bidentate ligands. For example, simple bipyridyl complexes of Pt(II) are rarely significantly luminescent in solution because they are unstable with respect to a D_{2d} distortion, namely a twisting of the plane of the N^N ligand relative to that of the other two ligating atoms, away from the square-planar configuration preferred by the d^8 ground state and towards a pseudo-tetrahedral geometry.[10] Such distortion facilitates non-radiative decay by promoting coupling with the ground state.[11] In contrast, complexes with tridentate ligands that form two 5- or 6-membered chelate rings have a strong preference for a planar geometry: there is little scope for D_{2d} distortion. In the case of the well-known tridentate *N^N^N*-coordinating ligand terpyridine (tpy), however, the bite angle is not ideal and the consequently weak ligand field leads to low-lying d-d states that deactivate the metal-to-ligand charge-transfer (MLCT) states: $[Pt(tpy)Cl]^+$ (Fig. 1)[12] is thus only *very* weakly luminescent at ambient temperature.[1a] The use of related ligands that form 6-membered chelates

can be beneficial, as they offer a bit angle closer to the desirable value of 180º.[13] Cyclometallating analogues of terpyridine, such as the isomeric *N^C^N*- and *N^N^C*-coordinating ligands 2,6-dipyridylbenzene and 6-phenyl-2,2'-bipyridine (phbpy, Fig. 1) respectively, are also superior in that the synergistic combination of a strongly σ-donating metallated aryl ring and π-accepting heterocycle leads to a large ligand field, pushing up the energy of d-d states and rendering them thermally less accessible at room temperature.[14,15,16] Nevertheless, the most reliable routes to such ligands rely upon cross-coupling chemistry and the associated use of relatively costly metallo-organic precursors and palladium catalysts, which reduce the attractiveness for scale-up.

The use of anionic phenolate donors in combination with neutral N-heterocycles or imines – as opposed to cyclometallating ligands – has emerged as a potentially interesting alternative. For example, the ligand salen, *N,N'*-bis(salicylidene)-1,2-ethylenediamine – well-known for its many catalytically active 1st row transition metal complexes – forms a highly luminescent Pt(II) complex,[17] as do related tetradentate ligands based on bipyridines and phenanthrolines (Fig. 1).[18] Meanwhile, with tridentate ligands, a range of luminescent *N^N^O*-coordinated Pt(II) complexes based on 6-(*o*-phenoxy)-2,2'-bipyridine have been reported (Fig. 1).[19, 20] Note that they feature one 5- and one 6-membered chelate ring.

In this contribution, we describe the results of our investigations into a new family of Pt(II) complexes incorporating tridentate *N^N^O*-coordinating Schiff-base ligands, which incorporate a 5-membered *N^N* chelate and a 6-membered *N^O* chelate. These ligands are based on either aromatic imines –C=N–Ar or hydrazones –C=N–N(R)–Ar (R = H or Me). Compared with ligands based on bipyridines and related cyclometallating ligands, they are very easily synthesised from low-cost, readily available starting materials, in high yield and in only one or two simple steps. Subsequent complexation to Pt(II) is achieved under milder conditions than those required for cyclometallating ligands. The photophysical properties of the complexes have been evaluated, some of them displaying quite intense phosphorescence in solution at ambient temperature.

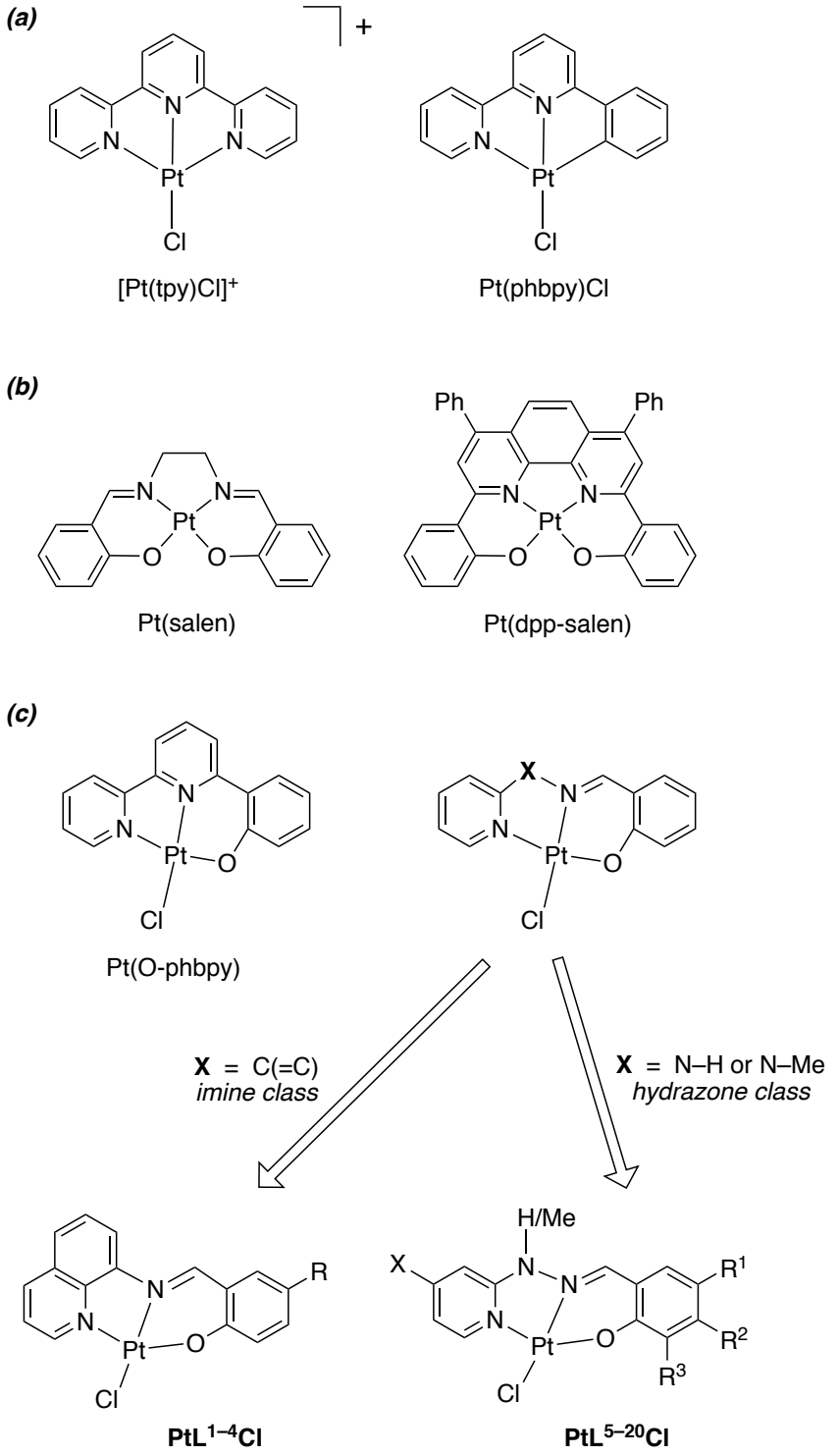

Figure 1 *(a) Pt(II) complexes of N^N^N-coordinating terpyridine [Pt(tpy)Cl]$^+$ and N^N^C-coordinating 6-phenyl-bipyridine Pt(phbpy)Cl.[12,14] (b) The O^N^N^O-coordinated Pt(II) complex of salen and an example of a related salen-like system based on 4,7-diphenyl phenanthroline Pt(dpp-salen).[16,17] (c) The Pt(II) complex of 6-(ortho-phenoxy)bipyridine Pt(O-phbpy)[18,19] and the generic structures of the two classes of N^N^O-coordinated Pt(II) complexes reported in this work (substitution patterns for the individual complexes are given in Fig. 2).*

RESULTS AND DISCUSSION

(i) Ligand design, synthesis, and complexation

Imine-based ligands HL^1–HL^4

We targeted *N^N^O*-coordinating tridentate proligands that would offer the metal centre a combination of a lateral pyridine or quinoline N donor, a central imine or hydrazone N donor, and a phenol or naphthol OH to bind via deprotonation (Fig. 1c). The ligand 8-(quinolyl)-salicylaldimine HL^1 (Scheme 1) was reported almost 40 years ago by Dahl and Dahl, who prepared a number of 1:2 (M:L) complexes of it with divalent 1st row transition metal ions, M = Mn^{2+}, Fe^{2+}, Co^{2+}, Ni^{2+}, Zn^{2+}.[21] Only with Cu^{2+} were square-planar complexes formed, of the structure Cu(*N^N^O*-L^1)X (X = Br or Cl). The authors' attempt to prepare the corresponding Pd(II) complex led to ligand hydrolysis, and they concluded that "palladium(II), having a lower affinity for oxygen compared to nitrogen, will possibly not use the oxygen donor atom for coordination". Despite their lack of success with Pd(II), we reasoned that the Pt(II) complex of such a ligand – if it could be synthesised – might display attractive photoluminescence properties.

In their study, Dahl and Dahl prepared HL^1 by condensation of 8-aminoquinoline and salicylaldehyde in "methanolic media". In our hands, the use of anhydrous methanol or ethanol consistently returned mixtures of the desired imine product with the starting materials, suggesting that the imine is prone to hydrolysis with an equilibrium being reached. It proved more effective to carry out the reaction under solvent-free conditions: the two reagents were mixed and heated with stirring at 65°C for 2 h under dynamic vacuum ($p < 5 \times 10^{-2}$ mbar, Scheme 1). ^{1}H NMR analysis showed almost complete conversion to the imine. Since purification attempts to obtain elementally pure material consistently still showed the presence of small traces of the aldehyde, apparently due to the ease of hydrolysis, the proligand was used in the subsequent complexation directly. A mixture of Pt(COD)Cl_2, anhydrous NEt_3 (excess) and anhydrous acetonitrile was added and the solution heated at reflux for 18 h. The desired complex PtL^1Cl precipitated from solution as a red

solid. Three other ligands $HL^{2–4}$ containing -OMe, -OCF_3, or -F respectively, *para* to the phenolic oxygen, were synthesised similarly and converted directly to their PtL^nCl complexes (Scheme 1). The identity of the complexes was confirmed by ^1H and ^{13}C NMR spectroscopy and by mass spectrometry. The absence of the OH proton in the ^1H NMR suggests that the phenolate oxygen is indeed bound to the metal, and this is confirmed in the solid state by an X-ray diffraction study of PtL^1Cl (discussed later).

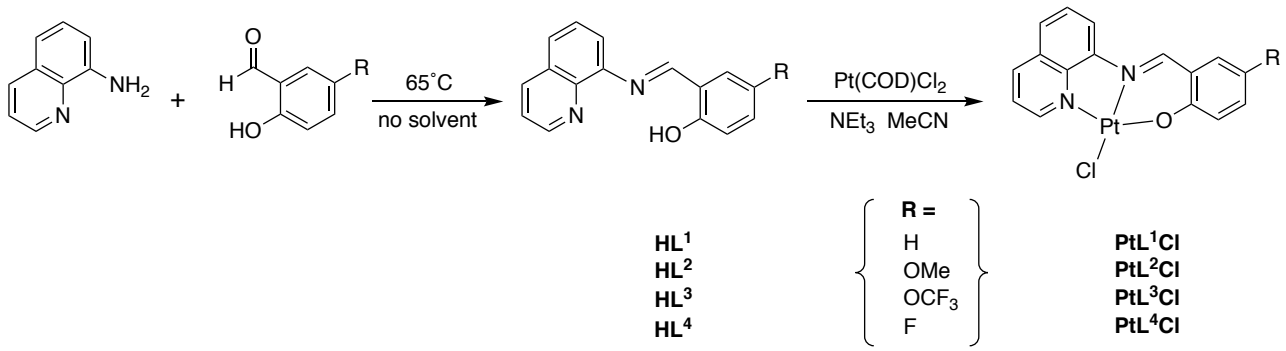

Scheme 1 *Synthesis of imine-based ligands $HL^{1–4}$ and their Pt(II) complexes $PtL^{1–4}Cl$.*

Hydrazone-based ligands HL^5–HL^{20}

These ligands (Scheme 2a,b) are structurally similar Schiff-base ligands to $HL^{1–4}$, again offering potential *N^N^O*-coordination through a combination of 5- and 6-membered chelate rings, but they are based on a hydrazone as opposed to imine linker. Sarkar and Pal reported oxovanadium(IV) complexes of *N*-(2-pyridyl)-*N*'-(salicylidene)hydrazine HL^5 and selected derivatives: they isolated complexes of the form V=O(*N^N^O*-L^5)(acac), in which L^5 is coordinated to the vanadium centre in a tridentate fashion through deprotonation of the phenol.[22] In contrast, the cobalt(II) complexes that have been reported are of the form Co(*N^O*-L^5)Cl(PPh_3), with the ligand bound in a bidentate as opposed to tridentate manner.[23] Six-coordinate complexes of type ML^5_2 with M = Zn(II), Cd(II) and Co(III) have recently been reported, while our own work was in progress.[24] We have prepared and investigated four-coordinate Pt(II) complexes of this ligand and a number of derivatives variously substituted in the phenol ring (Scheme 2a), together with analogues in which the ionisable hydrazone proton is replaced by a methyl group (Scheme 2b).

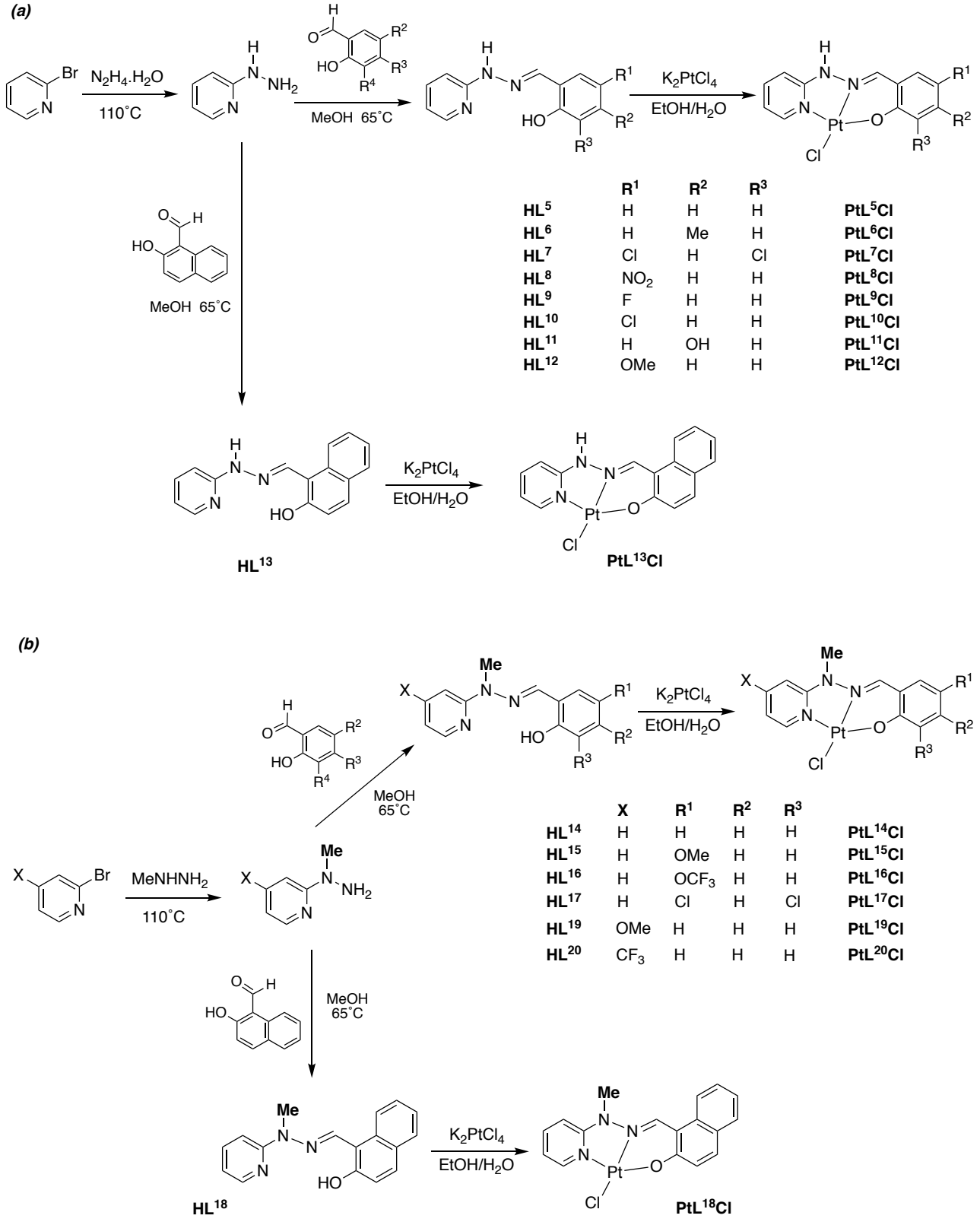

	R¹	R²	R³	
HL⁵	H	H	H	**PtL⁵Cl**
HL⁶	H	Me	H	**PtL⁶Cl**
HL⁷	Cl	H	Cl	**PtL⁷Cl**
HL⁸	NO_2	H	H	**PtL⁸Cl**
HL⁹	F	H	H	**PtL⁹Cl**
HL¹⁰	Cl	H	H	**PtL¹⁰Cl**
HL¹¹	H	OH	H	**PtL¹¹Cl**
HL¹²	OMe	H	H	**PtL¹²Cl**

	X	R¹	R²	R³	
HL¹⁴	H	H	H	H	**PtL¹⁴Cl**
HL¹⁵	H	OMe	H	H	**PtL¹⁵Cl**
HL¹⁶	H	OCF_3	H	H	**PtL¹⁶Cl**
HL¹⁷	H	Cl	H	Cl	**PtL¹⁷Cl**
HL¹⁹	OMe	H	H	H	**PtL¹⁹Cl**
HL²⁰	CF_3	H	H	H	**PtL²⁰Cl**

Scheme 2 *(a) Synthesis of hydrazone-based ligands $HL^{5–13}$ and their Pt(II) complexes $PtL^{5–13}Cl$. (b) Synthesis of related N-methyl-hydrazone ligands $HL^{14–20}$ and their Pt(II) complexes $PtL^{14–20}Cl$.*

The parent ligand HL^5 was synthesised by condensation of 2-hydrazinopyridine and salicylaldehyde in methanol at reflux, the former being readily prepared in high yield upon treatment of 2-bromopyridine with hydrazine hydrate (Scheme 2a). Derivatives $HL^{6–12}$, carrying various substituents in the phenol ring, were prepared similarly from the correspondingly substituted salicylaldehyde, whilst a naphthol analogue HL^{13} was also prepared from 2-hydroxy-naphthaldehyde. Related ligands $HL^{14–18}$ based on methylhydrazones (*i.e.*, in which the N–H is replaced by N–Me) were prepared similarly by initial reaction of 2-bromopyridine with methylhydrazine followed by condensation with the appropriate salicylaldehyde (for $HL^{14–17}$) or naphthaldehyde (HL^{18}) (Scheme 2b). We also synthesised two derivatives of the parent ligand that incorporate an electron-donating OMe or withdrawing CF_3 substituent *para* to the nitrogen of the pyridine ring, HL^{19} and HL^{20} respectively.

The Pt(II) complexes of these hydrazone ligands $PtL^{5–20}Cl$ were readily prepared upon treatment with K_2PtCl_4 in an ethanol / water mixture at reflux for 4 h. The desired complexes precipated from solution and were isolated by filtration and purified by recrystallisation from hot DMF. In appearance, the complexes are varying shades of yellow or green. Their identity was confirmed by ^1H and ^{13}C NMR spectroscopy, mass spectrometry and – for eight of the complexes – by X-ray crystallography (*vide infra*). In the ^1H NMR spectra, the most diagnostic indication of complexation was a significant shift of the N=C–H proton to high frequency, larger for the N–Me complexes than their N–H analogues. For example, for the N-methylated parent ligand HL^{14} in d_6-DMSO, δ_H = 8.05 ppm shifts to 8.94 ppm in the complex $PtL^{14}Cl$, compared to values of 8.29 and 8.61 ppm for the (non-methylated) HL^5 and PtL^5Cl respectively.

Chloride metathesis

It is well-established in the chemistry of $[Pt(tpy)X]^+$ and Pt(phbpy)X complexes that the change from X = Cl to a σ-donating acetylide X = –C≡C–Ar can augment luminescence efficiency by

increasing the total ligand field strength at the metal.[25,26,27] We therefore prepared two representative acetylide complexes, one of each class (imine and hydrazone), namely PtL^1-C≡C-Ar and PtL^{14}-C≡C-Ar where Ar = 3,5-bis(trifluoromethyl)benzene (Scheme 3). They were obtained by stirring a mixture of PtL^1Cl or $PtL^{14}Cl$, 3,5-bis(trifluoromethyl)phenylacetylene, NEt_3 and CuI in CH_2Cl_2 at 40°C for 48 h. The crude products were purified chromatographically to give the acetylide adducts as red and yellow solids, respectively.

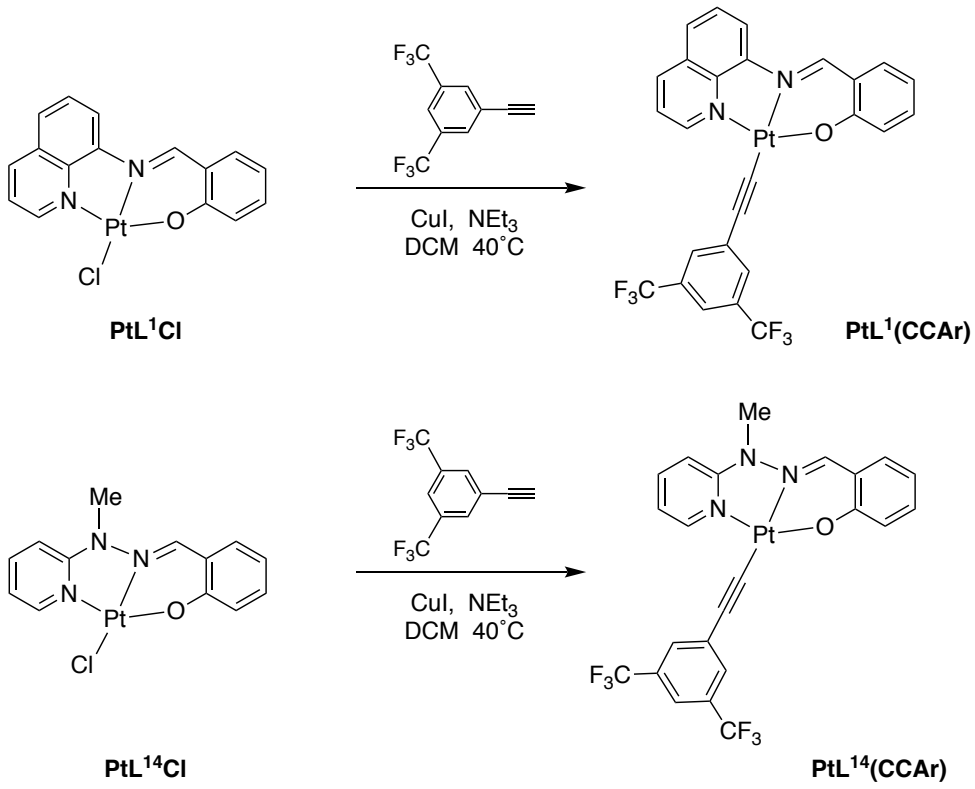

Scheme 3 *Substitution of the chloride ligand of PtL^1Cl and $PtL^{14}Cl$ by 3,5-bis(trifluoromethyl)-phenylacetylide to give PtL^1-C≡C-Ar and PtL^{14}-C≡C-Ar.*

(ii) Solid-state structures

Details of the crystallisation conditions, crystals, and refinement procedures are given in the Experimental Section and the Supporting Information (Table S1). All of the studied complexes show the expected square-planar coordination of the Pt(II) atom (examples are shown in Figs 2 and 3 with other complexes in Fig. S1 in the Supporting Information; selected bond lengths and angles involving the metal are summarised in Tables 1 and 2). The presence of extended conjugated

ligands results in a predominance of π···π interactions in the packing motifs. Anti-parallel complexes form stacks (dimers in the case of $PtL^{14}Cl$) with various degrees of slippage between adjacent molecules. The mutual orientation of the stacks varies and is probably dependent on the interactions between the metal complex molecules and solvent molecules which are present in all of the studied compounds except for $PtL^{14}Cl$ and $PtL^{19}Cl$. The N-H···O(solvent) hydrogen bonds are present in all the imine-based complexes. There are no short Pt···Pt separations of a magnitude (< 3.5 Å) that would indicate significant metal–metal interactions as found in some Pt(II) structures.[28] Typical molecular geometry and packing motifs are shown in Figs 2 and 3.

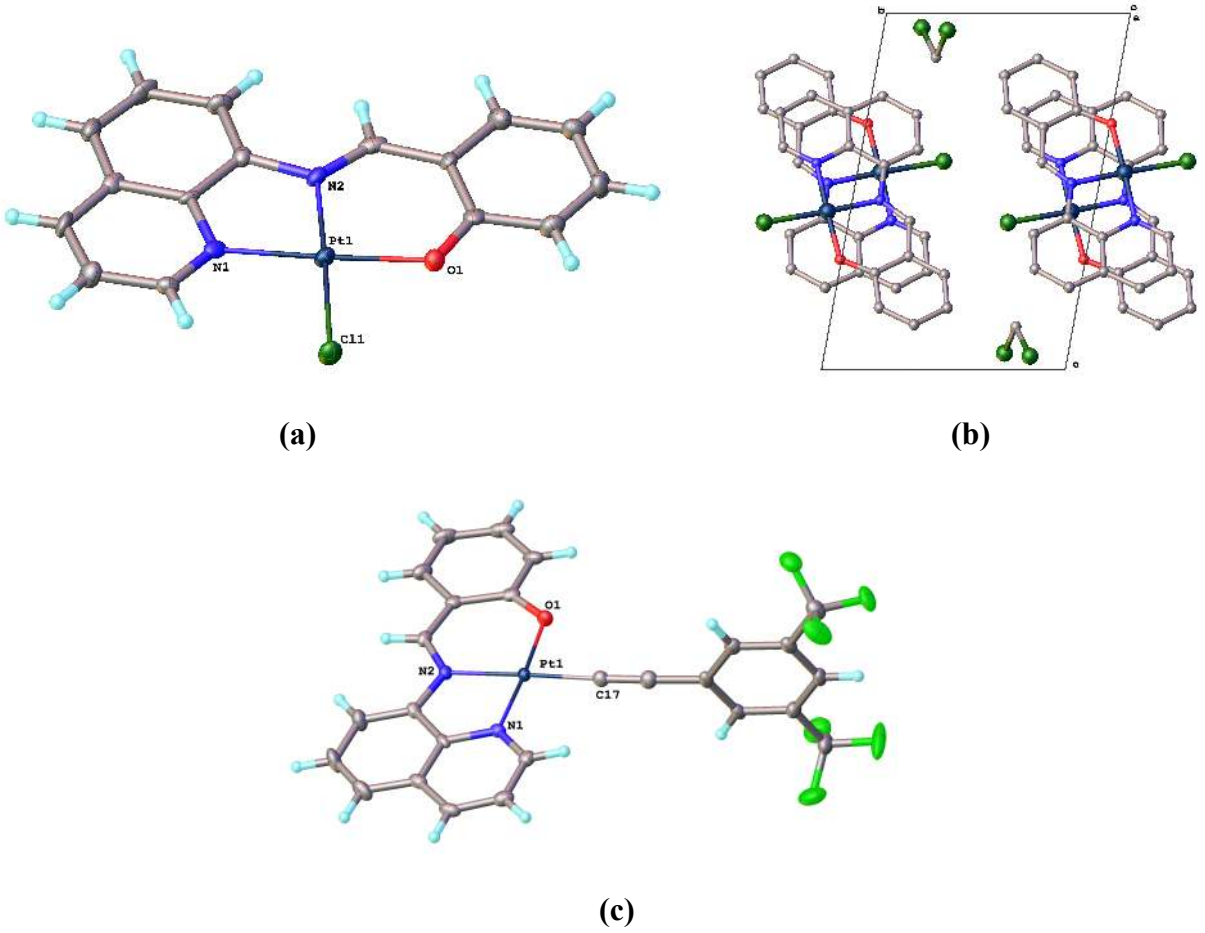

Figure 2 *(a) The molecular structure of $PtL^{1}Cl$ and (b) the packing of molecules within the crystal (view along the a-axis, H atoms omitted for clarity). (c) The molecular structure of PtL^{1}-C≡C-Ar.*

Table 1 Selected bond lengths, angles, and intermolecular Pt···Pt distances in PtL^1Cl and in PtL^1-C≡C-Ar determined by X-ray diffraction analysis of crystals at 120 K.

Bond lengths, angles, distances	**PtL^1Cl**	**PtL^1-C≡C-Ar**
$Pt–N^{quin}$ / Å	1.998(5)	1.993(2)
$Pt–N^{imine}$ / Å	1.971(5)	2.013(2)
Pt–O / Å	1.992(4)	1.997(2)
Pt–X / Å *(a)*	2.326(1)	1.966(3)
N^{quin}–Pt–O / °	177.4(2)	175.8(1)
N^{imine}–Pt–X / ° *(a)*	178.1(2)	178.5(1)
N–Pt–N / °	82.8(2)	82.0(1)
N–Pt–O / °	94.9(2)	93.8(1)
Pt···Pt short / Å	3.600	3.587
Pt···Pt long / Å	5.618	7.216

(a) X is the atom *trans* to the imine nitrogen: Cl for PtL^1Cl and C for PtL^1-C≡C-Ar.

Considering first the imine-based complex PtL^1Cl (Figure 2a,b and Table 1), the longest metal–ligand bond is, as would expected, that to the monodentate chloride ligand, 2.326(1) Å. The Pt–O and $Pt–N^{quin}$ bond lengths are the same within the experimental uncertainty {1.992(4) and 1.998(4) Å} whilst the central $Pt–N^{imine}$ is only marginally shorter. This pattern is similar to that for Pt(O-phbpy)Cl, which has a very similar set of bond lengths.[20] It contrasts with platinum(II) terpyridyl complexes, where the bond to the central N atom is normally shorter than those to the lateral nitrogen donors; *e.g.,* for $[Pt(tpy)Cl]^+$ in its triflate salt, the former is 1.930(4) Å compared to an average of 2.024 Å for the latter.[29] The combination of one 5- and one 6-membered chelate ring, as opposed to two 5-membered rings in tpy, relieves the strain and allows shorter bonds to form.

The molecular structure of PtL^1-C≡C-Ar is very similar to that of PtL^1Cl (Fig. 2c and Table 1). The $Pt–N^{imine}$ bond in the acetylide adduct is somewhat lengthened relative to the value in PtL^1Cl {2.013(2) versus 1.966(3) Å}, no doubt due to the greater *trans* influence of σ-donating acetylide

compared to chloride. Similar trends arising from acetylide substitution of chloride have been observed in platinum terpyridyl complexes.[30]

Crystals of N–H hydrazone complexes $PtL^{6}Cl$, $PtL^{8}Cl$ and $PtL^{12}Cl$ and of N-methyl hydrazone complexes $PtL^{14}Cl$, $PtL^{17}Cl$, $PtL^{19}Cl$ and $PtL^{20}Cl$ were obtained (as summarised in the Experimental Section) and analysed by X-ray diffraction. The structures of these hydrazone-based complexes are similar to that of the imine $PtL^{1}Cl$. One example each of an N–H and N–Me hydrazone structure is provided in Figures 3a and b respectively, and selected bond lengths and angles for all seven complexes are listed in Table 2 (see Fig. S1 for structures of other complexes). The central Pt–N^{hyd} bond is in all cases a little shorter than the lateral Pt–N^{py} and Pt–O bonds, which contrasts with the imine complexes where the difference was essentially insignificant. Otherwise, the bond lengths are similar to corresponding bonds in the imine complexes.

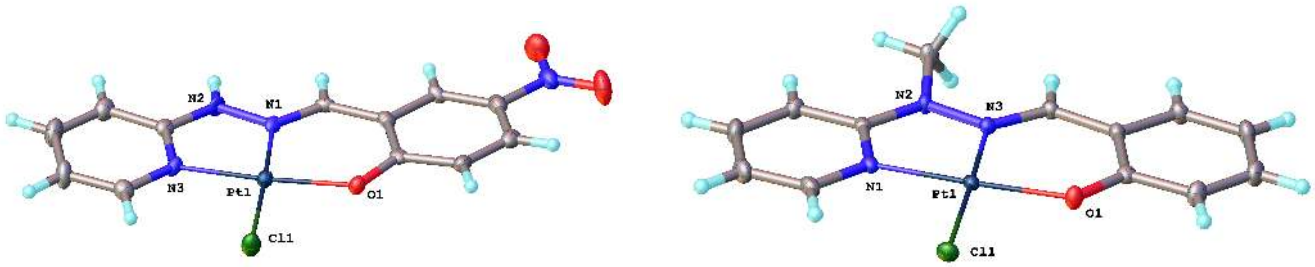

(a) **(b)**

Figure 3 *The molecular structures of (a) a representative N–H hydrazone complex, $PtL^{8}Cl$, and (b) a representative N-methyl-hydrazone complex, $PtL^{14}Cl$.*

Table 2 Selected bond lengths, angles, and intermolecular Pt···Pt distances in the Pt(II) complexes of hydrazone-based ligands, determined by X-ray diffraction analysis of crystals at 120 K.

Bond lengths, angles, distances	***N–H hydrazones***			***N–Me hydrazones***			
	$PtL^{6}Cl$	**$PtL^{8}Cl$**	**$PtL^{12}Cl$**	**$PtL^{14}Cl$**	**$PtL^{17}Cl$**	**$PtL^{19}Cl$**	**$PtL^{20}Cl$**
Pt–N^{py} / Å	1.995(4)	1.992(4)	1.994(2)	1.988(1)	1.977(2)	1.986(3)	1.979(3)
Pt–N^{hyd} / Å	1.953(4)	1.951(4)	1.941(2)	1.952(1)	1.960(2)	1.956(3)	1.959(3)
Pt–O / Å	1.981(3)	1.993(3)	1.990(2)	1.976(1)	1.985(2)	1.989(2)	1.980(2)
Pt–Cl / Å	2.310(1)	2.295(1)	2.303(7)	2.305(1)	2.307(1)	2.311(1)	2.307(1)
N^{py}–Pt–O / °	175.6(2)	175.4(2)	175.7(1)	176.6(1)	176.5(1)	176.3(1)	177.0(1)
N^{hyd}–Pt–Cl / °	178.3(1)	177.3(1)	177.6(1)	177.6(1)	177.1(1)	177.6(1)	177.8(1)
N–Pt–N / °	81.6(2)	81.2(2)	81.1(1)	81.0(1)	80.9(1)	81.1(1)	81.2(1)
N–Pt–O / °	94.0(2)	94.4(2)	94.6(1)	95.6(1)	95.6(1)	95.4(1)	95.7(1)
Pt···Pt / Å	5.948	5.070	5.222	5.177	4.398	4.733	4.660

(iii) Photophysical properties of imine-based complexes

UV-visible absorption spectra

The UV-visible absorption spectra of complexes $PtL^{1–4}Cl$ and PtL^{1}-C≡C-Ar were recorded in dichloromethane solution at room temperature (Fig. 4 and Table 3). The spectrum of $PtL^{1}Cl$ shows a set of very intense bands in the near-UV region, together with a broad, moderately intense band in the visible region, centred at 511 nm. The latter can reasonably be attributed to a charge-transfer transition in which the charge-accepting unit will be the quinoline π* orbitals. Low-energy MLCT bands are observed in the complexes of this ligand with some first-row metal ions such as Cu^{2+} and Ni^{2+},[21] whilst LMCT bands are lowest in energy in the d^0 dioxovanadium(V) complex.[31] In comparison, the corresponding proligand HL^{1} displays no bands in the visible region in apolar, non-hydrogen-bonding solvents like cyclohexane, although in MeOH and DMF a band appears at around 455 nm attributed to presence of the *o*-quinoid tautomeric form of HL^{1}, whose formation is favoured by solvents that can form hydrogen bonds.[21,32]

The spectra of $PtL^{2–4}Cl$ are very similar in form to that of $PtL^{1}Cl$, although the low-energy band is significantly red-shifted to 550 nm in the case of the methoxy-bearing complex $PtL^{2}Cl$ (Fig. 4a). This red-shift supports the charge-transfer assignment proposed above, as the electron-donating MeO substituent positioned *para* to the phenolate oxygen will serve to increase the electron density at the metal and the highest filled molecular orbitals. Indeed, density functional theory (DFT) calculations reveal the significant participation of the metal, the phenolate, and the chloride coligand in the HOMO (Fig. S2). The quinoline unit, in contrast, makes very little contribution to the HOMO, but it predominates in the LUMO; the transition may thus be best formulated as $d_{Pt} \mid \pi_{ArO-} \rightarrow \pi^*_{quin}$ or MLCT/LLCT in character.

The substitution of chloride by the arylacetylide ligand in PtL^{1}-C≡C-Ar does not significantly affect the profile of the spectrum, although the intensities of the bands in the UV region are increased throughout, and not just in the region where the π-π* transitions of the acetylide are expected to contribute to the spectrum (Fig. 4b).

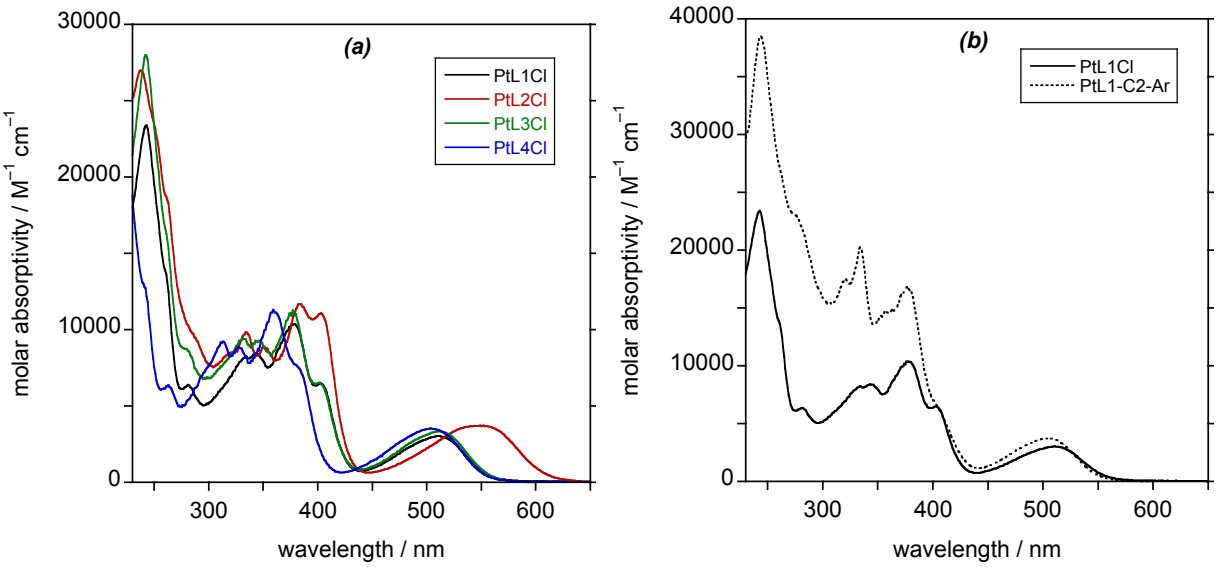

Figure 4 *UV-visible absorption spectra of (a) $PtL^{1–4}Cl$ in CH_2Cl_2 at 295 K and (b) the spectrum of PtL^{1}-C≡C-Ar overlaid with that of $PtL^{1}Cl$ under the same conditions.*

Photoluminescence properties

The imine complexes prove to be luminescent in solution at room temperature, confirming the original hypothesis that ligands of this type might allow the formation of phosphorescent Pt(II) complexes. In deoxygenated dichloromethane solution, PtL^1Cl emits in the deep red region, λ_{max} = 635 nm, displaying a vibrationally resolved spectrum in which the 0,0 component has the highest intensity (Fig. 5a and Table 3). Such a profile is typically associated with excited states with little structural distortion relative to the ground state.[33] The photoluminescence quantum yield was measured to be 0.04, making it similar to the paradigmatic $[Ru(bpy)_3]Cl_2$,[34] despite emitting to lower energy. Quantum yields of luminescent transition metal complexes invariably fall off towards the red region, in line with the energy gap law: the highest efficiencies are invariably found for green emitters such as *fac*-$Ir(ppy)_3$.[35]

The phosphorescent nature of the emission is evident from the long luminescence lifetime of 6.8 μs in deoxygenated solution at ambient temperature. The emission is strongly quenched by oxygen: the lifetime falls to 600 ns in air-equilibrated solution and the bimolecular rate constant for quenching by oxygen was calculated to be 6.8×10^8 M^{-1} s^{-1}.

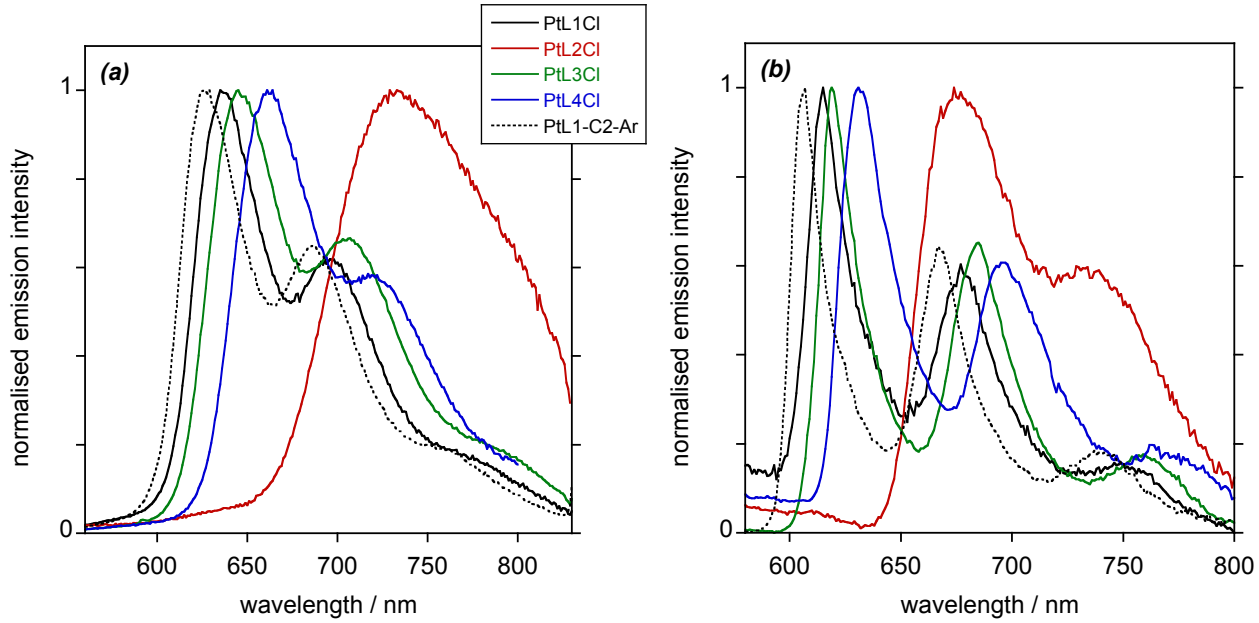

Figure 5 *(a) Emission spectra of $PtL^{1-4}Cl$ and PtL^1-C≡C-Ar in CH_2Cl_2 at 295 ± 1 K. (b) Emission spectra of the same complexes at 77 K in EPA (= diethyl ether / isopentane / ethanol, 2:2:1 v/v).*

Table 3 Photophysical data for $PtL^{1–4}Cl$ and PtL^{1}-C≡C-Ar, in CH_2Cl_2 at 295 ± 1 K except where otherwise stated.

Complex	Absorption at 298 K *(a)*	Emission at 298 K						Emission at 77 K *(b)*	
	λ_{max} / nm (ε / M^{-1} cm^{-1})	λ_{max} / nm	τ / ns *(c)*	Φ_{lum} × 10^2 *(d)*	k_r /10^3 s^{-1} *(e)*	$\sum k_{nr}$ /10^3 s^{-1} *(e)*	k_q^{O2} *(f)* /10^8 M^{-1} s^{-1}	λ_{max} / nm	τ / ns
$PtL^{1}Cl$	243 (23400), 281 (6390), 334 (8280), 346 (8390), 376 (10400), 402 (6470), 511 (3030)	635, 700	6800 [600]	4.0	5.9	140	6.8	615, 677, 755	14000
$PtL^{2}Cl$	238 (27000), 318 (8470), 334 (9830), 353 (8820), 385 (11700), 403 (6470), 550 (3680)	735	1800 [300]	0.5	2.8	550	13	677, 737	13000
$PtL^{3}Cl$	242 (28000), 280 (8740), 334 (9400), 346 (9290), 377 (11300), 401 (6540), 512 (3340)	645, 710	4500 [400]	2.2	4.9	220	10	619, 686, 762	11000
$PtL^{4}Cl$	284 (5740), 334 (8210), 348 (9320), 379 (7720), 403 (2000), 524 (2730)	660, 720	4800 [400]	2.9	6.0	200	10	631, 696, 766	13000
PtL^{1}-C≡C-Ar	244 (38500), 279 (22400), 320 (17500), 334 (20300), 378 (16700), 406sh (6200), 505 (3710)	627, 686	11000 [400]	4.6	4.3	90	11	607, 667, 741	20000

(a) Maxima at λ > 230 nm are listed. *(b)* In diethyl ether / isopentane / ethanol (2:2:1 v/v). *(c)* In diethyl ether / isopentane / ethanol (2:2:1 v/v). *(c)* Luminescence lifetimes in deoxygenated solution; values in parenthesis refer to air-equilibrated solutions. *(d)* Luminescence qunatum yield in deoxygenated solution, measured using $[Ru(bpy)_3]Cl_{2\ (aq)}$ as the standard. *(e)* k_r and $\sum k_{nr}$ are the radiative and non-radiative rate constants, estimated from the lifetime and quantum yield, assuming that the emitting state is formed with unitary efficiency: $k_r = \Phi_{lum} / \tau$; $\sum k_{nr} = (1–\Phi_{lum}) / \tau$. *(f)* Bimolecular rate constant for quenching by molecular oxygen estimated from the lifetimes in deoxygenated and air-equilibrated solution, and taking $[O_2]$ = 2.1 mmol dm^{-3} in CH_2Cl_2 at atmospheric pressure of air at 295 K.

The emission properties of PtL^3Cl and PtL^4Cl are very similar to those of PtL^1Cl (Fig. 5a and Table 3). There is a small red shift in the emission maxima in the order 1→3→4. On the other hand, the emission of PtL^2Cl is strongly red-shifted to λ_{max} = 735 nm, mirroring the trend observed in absorption. The vibrational structure is lost in this case, and the emission is substantially weaker and shorter-lived (Table 3). If it is assumed that the emissive state is formed with unitary efficiency, then the radiative k_r and non-radiative $\sum k_{nr}$ rate constants can be estimated through $k_r = \Phi / \tau$ and $\sum k_{nr} = (1 - \Phi) / \tau$. The values obtained in this way are compiled in Table 3: they suggest that the weaker and shorter-lived emission of PtL^2Cl is due to the combined effects of a lower k_r value as well as a higher k_{nr} value. The latter is expected on the basis of the so-called "energy gap law": within a given family of emitters, non-radiative decay by intermolecular energy transfer into vibrations increases as the excited-state energy decreases, due to more favourable Frank-Condon overlap of the vibrational wavefunctions.[36] The reduction in the phosphorescence decay rate constant k_r may reflect a decreasing degree of participation of the metal in the excited state, as the filled ligand-based orbitals rise in energy, in line with previous observations with red-emitting cyclometallated Pt(II) complexes for example.[37]

The emission properties of PtL^1-C≡C-Ar are quite similar to those of PtL^1Cl. There is, however, a small increase in the quantum yield and a larger increase in the lifetime: the value of $\sum k_{nr}$ is reduced by approximately one-third. It is well established that the replacement of halide ligands X by acetylides in complexes of the type $Pt(N^N)X_2$ and $[Pt(N^N^N)X]^+$ can have a beneficial effect on room-temperature emission quantum yields through a reduction in $\sum k_{nr}$.[38, 25-27] The effect arises from the increased ligand field which raises potentially deactivating d-d states to higher energy: thermally activated non-radiative decay of the emissive charge-transfer state via such metal-centred states is then inhibited. In the present instance, the influence is only modest, probably reflecting the low energy of the emissive excited state: the energy gap to the d-d states is already likely to be quite large even for chloride as the monodentate ligand. Related conclusions have been made for complexes of N^C^N-coordinating ligands, where the ligand field strength is already strong.[39]

The spectra recorded at 77 K are quite similar to those at room temperature (Fig. 5b). The vibrational structure is somewhat better resolved and the emission is modestly shifted to higher energy by about 500 cm^{-1} for PtL^1Cl, PtL^3Cl and PtL^4Cl. The blue-shift is larger for PtL^2Cl, consistent with a higher degree of charge-transfer character as postulated above.

(iv) Photophysical properties of hydrazone-based complexes

UV-visible absorption spectra: N–H hydrazone complexes

The UV-visible absorption spectra of complexes $PtL^{1–4}Cl$ and PtL^1-C≡C-Ar were recorded in solution in acetonitrile, which offered better solubility than dichloromethane and was more suitable for examination of the effect of deprotonation of the hydrazone. It is well-established that deprotonation of free hydrazones occurs only under highly basic conditions, but that coordination to a metal ion causes a significant increase in the acidity of the N–H proton.[40] Complexes of substituted hydrazones R^1–NH–N=CH–R^2 are known as colorimetric reagents and their acid-base behaviour is accompanied by remarkable colour changes.[41] Protonated and deprotonated forms can co-exist even in the crystalline state, for example, as reported for the Pd(II) complex of 2-(diphenylphosphine)benzaldehyde 2-pyridylhydrazone.[42]

The UV-visible spectra of the complexes (Table 4 and Fig. 6) feature an intense well-defined band in the visible region, centred between 409 and 442 nm according to the substituents, with evidence of a vibrational shoulder to high energy. These bands, together with those around 350 nm, are attributed to charge-transfer transitions associated with the introduction of the metal, as put forward by Mohan *et al.*[43] Evidence for the formation of the deprotonated system is provided by the influence of base on the UV-visible spectra. We selected the F-substituted complex PtL^9Cl for more detailed study of the effect of N–H deprotonation on the absorption spectrum (Fig. 6a). The initial, protonated form of the complex shows intense bands at 349 and 430 nm. Upon addition of triethylamine base, a new, very intense band appears centred at 453 nm, with accompanying large

increases in absorbance across the near-UV and visible regions. The new band is likely to be associated with the more extended charge delocalisation in the deprotonated system: the negative charge on the nitrogen atom can conjugate with the N=C-Ar unit (Scheme 4). There is a vivid colour change visible to the eye from an initial pale yellow to an intense bright yellow colour. The changes are reversible: the original spectrum could be recovered upon addition of acetic acid. The presence of well-defined isosbestic points in the titration – at 355, 306 and 297 nm – indicate that the deprotonation proceeds without formation of any other species.

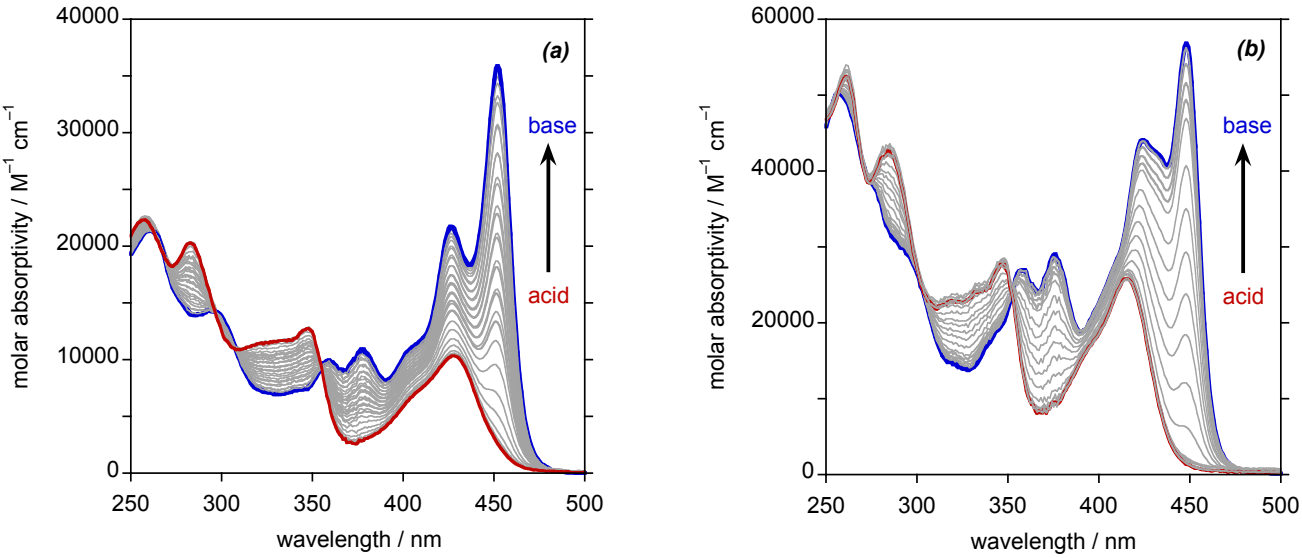

Figure 6 *UV-visible absorption spectra of (a) PtL^{9}Cl and (b) PtL^{8}Cl in MeCN at 295 K in the presence of CH_3CO_2H (red lines) and their evolution upon deprotonation of the hydrazone through addition of increasing quantities of triethylamine.*

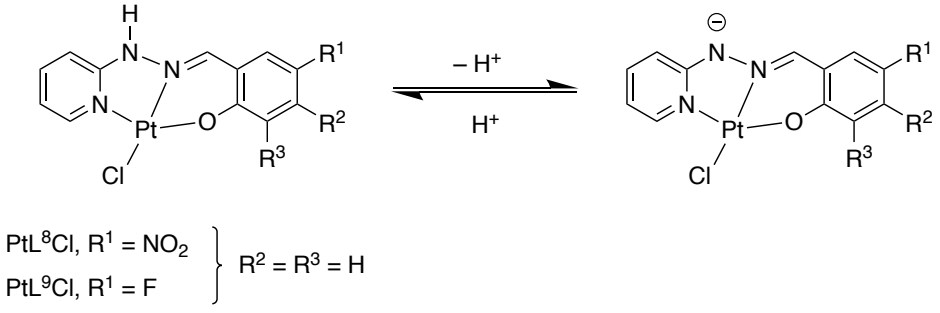

Scheme 4 *Deprotonation of the N–H hydrazone complexes PtL^{n}Cl (n = 5–13). The two examples shown – PtL^{8}Cl and PtL^{9}Cl – gave the clearest isobestic points amongst the series.*

Similar behaviour was observed for the nitro derivative PtL^8Cl (Fig. 6b), but the isosbestic points were less well-defined for other complexes in the series. It became apparent, however, that the complexes were sensitive to light-induced decomposition in solution, degrading over time, and accounting for the lack of clear isobestic points; PtL^9Cl and PtL^8Cl appeared to be the most robust systems. Even for PtL^9Cl, we noted gradual spectral changes when an acetonitrile solution was exposed to sunlight over a period of 6 h, with a concomitant rise in the baseline suggesting some precipitation of an insoluble degradation product (Supporting Information, Fig. S3). On the other hand, for an identical control solution kept in the dark, no change in the spectrum was observed.

Table 4 UV-visible absorption data in acetonitrile solution for N–H hydrazone complexes $PtL^{5–13}Cl$ and their deprotonated states formed through the addition of excess triethylamine.

Complex	**Protonated state**[(a)] λ_{max} / nm (ε / M^{-1} cm^{-1})	**Deprotonated state**[(b)] λ_{max} / nm (ε / M^{-1} cm^{-1})
PtL^5Cl	268 (28800), 280 (20500), 346 (9880), 417 (6750)	297 (14400), 358 (9400), 375 (10200), 423 (16400), 447 (22900)
PtL^6Cl	262 (24700), 285 (19700), 349 (12900), 417 (12600)	298 (13300), 358 (12000), 377 (12900), 425 (19800), 448 (25600)
PtL^7Cl	257 (25900), 285 (18000), 351 (11800), 429 (9710)	297 (14400), 359 (7740), 377 (8110), 428 (18800), 454 (33900)
PtL^8Cl	279 (21100), 338 (18700), 410 (15000), 448 (7630)	287 (11900), 351 (22100), 369 (25700), 426 (16900), 449 (23800)
PtL^9Cl	259 (18800), 284 (16800), 349 (11000), 430 (10200)	295 (12700), 361 (8500), 379 (9450), 427 (19200), 453 (31700)
$PtL^{10}Cl$	261 (26200), 284 (20000), 348 (12600), 426 (9300)	297 (14600), 358 (9150), 377 (9630), 426 (19500), 452 (32100)
$PtL^{11}Cl$	264 (21500), 289 (15700), 351 (11000), 409 (14500)	291 (15400), 357 (13600), 376 (13900), 430 (18800), 449 (18100)
$PtL^{12}Cl$	270 (20400), 287 (18400), 349 (13100), 442 (8190)	302 (14200), 365 (8860), 384 (10000), 433 (16600), 458 (26500)
$PtL^{13}Cl$	269 (33100), 334 (12400), 353 (12000), 441 (14800)	297 (23000), 378 (7840), 399 (8500), 441 (21900), 470 (33000)

(a) Spectra recorded in the presence of excess CH_3CO_2H to ensure that only the protonated form was present in solution. (b) Deprotonated forms were obtained *in situ* by addition of excess triethylamine until no further changes in the spectra were observed.

UV-visible absorption spectra: N–Me hydrazone complexes

The N-methylated hydrazone complexes $PtL^{14–20}Cl$ and PtL^{14}-C≡C-Ar show no variation in their UV-visible absorption spectra with added base or acid, nor do they show any evidence of light-activated degradation in solution. They are more soluble in CH_2Cl_2 than their N-H analogues. The absorption spectra in CH_2Cl_2 are shown in Figure 7: for clarity, the complexes with varying phenolate substituent are grouped in (a) and the derivatives with varying pyridyl substituent in (b). Numerical data are collated in Table 5. The similarity of the spectra to those of the protonated N-H forms of the previously discussed hydrazone complexes (Fig. 6) is clear.

The position of the lowest-energy band is influenced by the phenolate substituent. For example, in the complex carrying the *para*-methoxy substituent in the phenol ring $PtL^{15}Cl$, this band is shifted by about 1300 cm^{-1}, which would be consistent with a raising of the highest-energy filled orbitals – expected to be based on the phenolate and metal – with little effect on the lowest unoccupied orbitals – which might be expected to be based on the heterocycle. The naphthol analogue $PtL^{18}Cl$ also displays a red-shift in this band, consistent with the more extended conjugation in the ligand.

On the other hand, the introduction of an electron-donating OMe group into the *para* position of the pyridine ring in $PtL^{19}Cl$ is seen to lead to only a small red-shift of the low-energy band, whilst λ_{max} for the CF_3 derivative $PtL^{20}Cl$ is essentially the same as the parent (Fig. 7b). The relative lack of effect may reflect the fact that both of the frontier orbitals (HOMO *and* LUMO) are rather delocalised across the molecule (illustrated in Fig. S4 for $PtL^{14}Cl$), such that the substituents affect the energy of filled orbitals and not just the vacant orbitals. Finally, the replacement of the chloride ligand of $PtL^{14}Cl$ by an acetylide in PtL^{14}-C≡C-Ar has little effect on the positions of the bands, although as in PtL^{1}-C≡C-Ar, there is a general increase in molar absorptivity across the spectrum (Fig. S5).

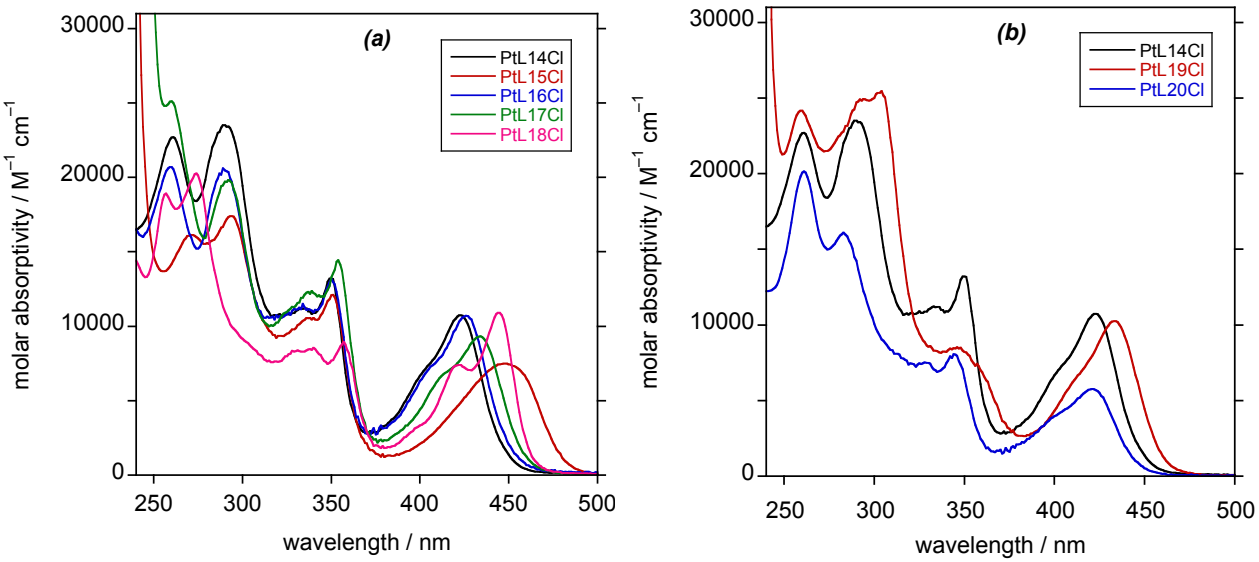

Figure 7 *UV-visible absorption spectra of (a) PtL$^{14–18}$Cl and (b) PtL$^{19–20}$Cl (with PtL^{14}Cl shown for ease of comparison), in CH_2Cl_2 at 295 K in each case.*

Photoluminescence properties

The N-methyl hydrazone complexes are luminescent in solution at ambient temperature (Table 5). They emit in the red region of the spectrum, displaying quite broad bands, though with a hint of structure to the high energy side in each case (Fig. 8). The phenolate substituents have a modest influence on the emission maximum (Fig. 8a), largely mirroring the trend observed in the absorption spectra. Thus, the emission maximum of the *para*-methoxyphenolate complex PtL^{15}Cl is displaced by around 1000 cm^{-1} to lower energy compared to the parent PtL^{14}Cl, and the more conjugated naphtholate complex PtL^{18}Cl is similarly red-shifted. As in absorption, the introduction of a *para*-OMe or *para*-CF_3 substituent into the pyridine ring has almost negligible effect (Fig. 8b). The quantum yields are mostly in the range 1–2% with lifetimes of the order of a microsecond. However, the introduction of the acetylide ligand in PtL^{14}-C≡C-Ar is seen to substantially boost the quantum yield to 11%, with a concomitant increase in the lifetime (Fig. 8c). It is evident from the kinetic parameters listed in Table 5 that this outcome is due almost exclusively to an approximately 5× reduction in $\sum k_{nr}$. It seems likely that an effect comparable to that found in platinum terpyridyl

acetylide complexes is at work, with the strong ligand field helping to reduce deactivation through higher-lying metal-centred states.[25-27] Conversely, the naphtholate complex Pt[18]Cl displays notably weaker emission, apparently due largely to a reduced k_r value. The tendency to lower triplet radiative rate constants in metal complexes as ligand conjugation increases has been reported elsewhere, and probably stems from a decrease in metal character in the excited state as the energy of filled metal orbitals rises with increasing conjugation.[37,44]

At higher concentrations in CH_2Cl_2 (values in the range $3 \times 10^{-6} - 5 \times 10^{-5}$ M were examined), there was no significant reduction in the lifetime, nor did any low-energy emission band appear that might be attributable to excimer formation. This contrasts with many reported *N^C^N*-coordinated Pt(II) complexes, for example, which show a strong propensity to excimer formation. It also contrasts with the behaviour of *N^N^C*-coordinated complexes based on phenylbipyridines,[15] as well as many Pt(*N^N^N*) systems,[25,45] where metal–metal interactions at elevated concentrations can lead to low-energy absorbing and emitting MMLCT states. In this respect, it is noteworthy to recall that the crystal structures show no close Pt···Pt contacts. Evidently, the preferred orientation of the molecules, at least in the crystals, does not involve metal–metal interactions.

In a frozen dilute glass at 77 K, the vibrational structure becomes well resolved (see Fig. 8d for PtL[14]Cl as a representative example and Fig. S6 for other complexes). The trend in the wavelength of the 0,0 band follows that of λ_{max} at room temperature.

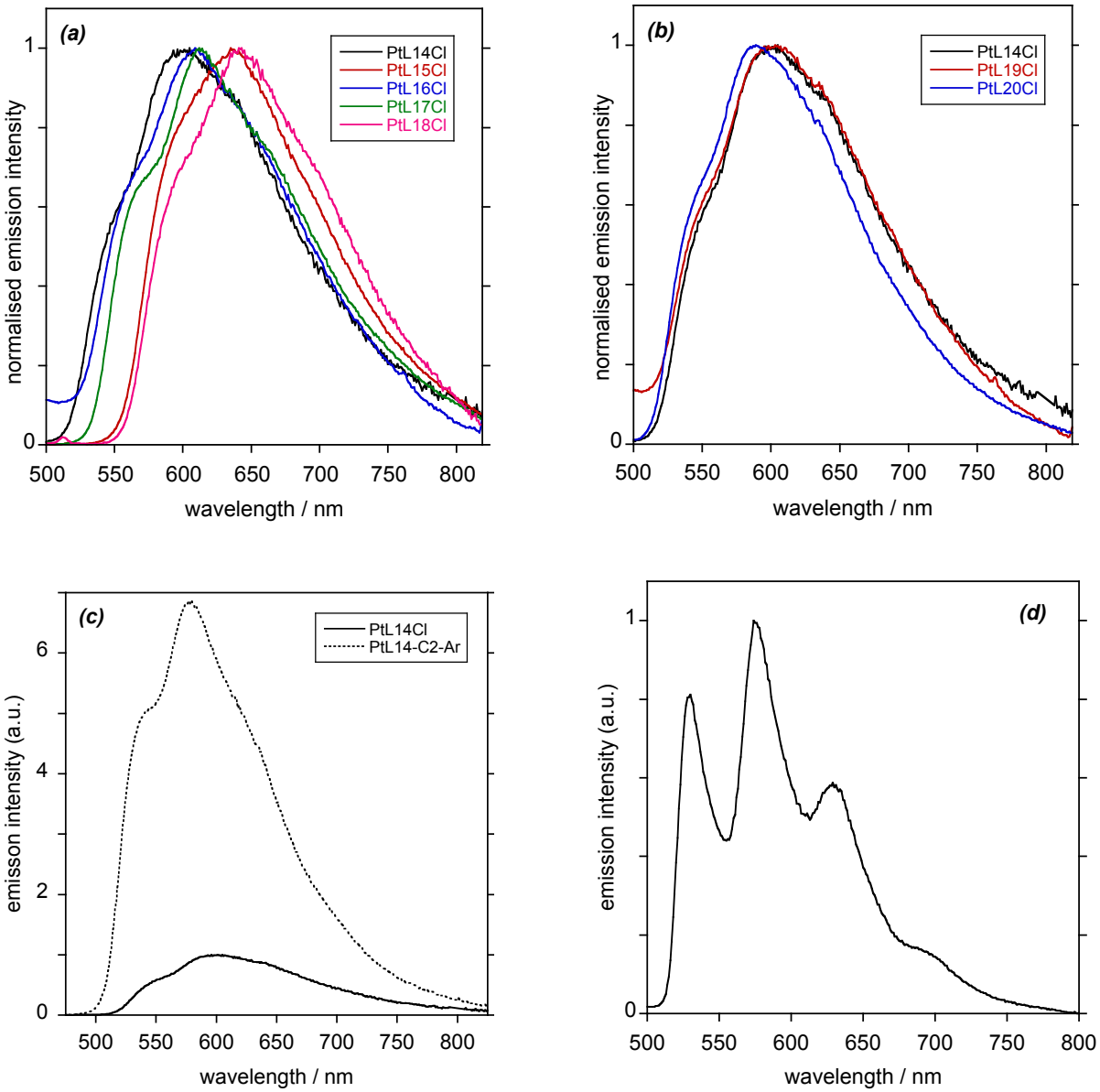

Figure 8 *Normalised emission spectra of (a) PtL$^{14–18}$Cl and (b) PtL$^{19–20}$Cl (with PtL^{14}Cl shown for ease of comparison), in CH_2Cl_2 at 295 K in each case. (c) Emission spectra of PtL^{14}Cl and PtL^{14}-C≡C-Ar isoabsorbant at the excitation wavelength of 420 nm, showing the beneficial effect of the acetylide ligand on emission efficiency. (d) The emission spectrum of PtL^{14}Cl at 77 K in EPA; the corresponding 77 K spectra of all other complexes are shown in Fig. S6.*

Table 5 Photophysical data for $PtL^{14–20}Cl$ and PtL^{14}-C≡C-Ar, in CH_2Cl_2 at 298 ± 3 K except where otherwise stated.

Complex	Absorption at 298 K	Emission at 298 K						Emission at 77 K *(a)*	
	λ_{max} / nm (ε / M^{-1} cm^{-1})	λ_{max} / nm *(b)*	τ / ns *(c)*	Φ_{lum} × 10^2 *(d)*	k_r /10^3 s^{-1} *(e)*	$\sum k_{nr}$ /10^3 s^{-1} *(e)*	k_q^{O2} *(f)* /10^8 M^{-1} s^{-1}	λ_{max} / nm	τ / ns
$PtL^{14}Cl$	261, 292, 333, 350, 399sh, 423	550sh, 599	2100 [400]	1.7	8.1	470	9.2	529, 575, 628	36000
$PtL^{15}Cl$	274, 294, 339, 351, 448	593sh, 636	3400 [200]	1.5	4.4	290	2.1	564, 614, 674	39000
$PtL^{16}Cl$	261, 286, 335, 351, 403sh, 427	563sh, 609	2300 [400]	1.4	6.1	430	9.4	540, 589, 645	40000
$PtL^{17}Cl$	261, 293, 338, 354, 412sh, 434	568sh, 613	2300 [300]	1.2	5.2	430	1.2	545, 594, 653	36000
$PtL^{18}Cl$	257, 274, 330, 340, 357, 422, 444	596sh, 641	1500 [400]	0.4	2.7	660	8.3	575, 628, 689	23000
$PtL^{19}Cl$	259, 294, 304, 349, 410sh, 435	547sh, 600	1800 [300]	1.7	9.4	540	1.3	528, 573, 627	41000
$PtL^{20}Cl$	261, 283, 331, 346, 398sh, 422	540sh, 589	2000 [300]	2.1	11	490	1.3	529, 576, 629	49000
PtL^{14}-C≡C-Ar	260, 297, 338, 353, 399sh, 420	542sh, 580	9300 [400]	11	12	90	1.1	523, 568, 620	55000

(a) In diethyl ether / isopentane / ethanol (2:2:1 v/v). *(b)* The spectra are less well resolved than those of the imine complexes, where the 0,0 vibrational component band could be unequivocally identified. In the present case, the high energy shoulder indicated likely approximates to the 0,0 transition. *(c)* Luminescence lifetimes in deoxygenated solution; values in parenthesis refer to air-equilibrated solutions. *(d)* Luminescence qunatum yield in deoxygenated solution, measured using $[Ru(bpy)_3]Cl_{2\ (aq)}$ as the standard. *(e)* k_r and $\sum k_{nr}$ are the radiative and non-radiative rate constants, estimated from the lifetime and quantum yield, assuming that the emitting state is formed with unitary efficiency: $k_r = \Phi_{lum} / \tau$; $\sum k_{nr} = (1–\Phi_{lum}) / \tau$. *(f)* Bimolecular rate constant for quenching by molecular oxygen estimated from the lifetimes in deoxygenated and air-equilibrated solution, and taking $[O_2]$ = 2.1 mmol dm^{-3} in CH_2Cl_2 at atmospheric pressure of air at 295 K.

As to the N–H hydrazone complexes, no firm conclusions can be drawn regarding their emissive properties owing to their sensitivity to light and the apparent degradation under irradiation. However, weak emission was observed for PtL^6Cl in deoxygenated acetonitrile solution at room temperature, with a spectral profile similar to that of its N-methyl hydrazone analogue $PtL^{14}Cl$ (Fig. S7). The quantum yield of 0.3% is significantly reduced, however, consistent with there being an additional deactivation pathway involving irreversible degradation. Upon deprotonation of the complex through addition of base, the emission is red-shifted and further reduced in intensity (Fig. S7).

Concluding remarks

In summary, the use of simple Schiff base chemistry to link pyridyl and phenolate rings via a central N atom generates *N^N^O*-coordinating tridentate ligands that can be used to access new luminescent platinum(II) complexes of the form Pt(*N^N^O*)Cl under mild conditions. These molecular materials are phosphorescent in the red region of the spectrum in solution at ambient temperature. The class of complex based on imine linkers, derived from 8-aminoquinoline, are mostly somewhat superior to those based on hydrazones: they have rather higher quantum yields and longer lifetimes, despite emitting more deeply in the red, due to lower non-radiative decay constants. Further improvements in the quantum yield can be obtained for each class by replacing the chloride coligand by an acetylide, the effect being more significant for the hydrazone case than the imine analogue. A further interesting feature of the imine complexes is the presence of an intense low-energy absorption band at $\lambda_{max} \sim 520$ nm. The hydrazone complexes featuring an N–H unit suffer from photodecomposition leading also to poor emission quantum yields, but the use of an analogous N-methylated linker circumvents this problem, leading to superior performance. These readily accessed Schiff-base ligands may provide interesting alternatives to ligands based on terpyridines and aryl-bipyridines in the future development of new triplet-emitting molecular materials.

EXPERIMENTAL DETAILS

General

Reagents were obtained from commercial sources and used without further purification unless stated otherwise. All solvents used in preparative work were at least Analar grade and water was purified using the Purite$_{STILL}$ plus^{TM} system. ^{1}H and ^{13}C NMR spectra were recorded on a Bruker Avance-400 spectrometer. Two-dimensional NMR (COSY, NOESY, HSQC and HMBC) spectra were acquired on Varian VNMRS-600 (600 MHz) or VNMRS-700 (700 MHz) instruments. Chemical shifts (δ) are in ppm, referenced to residual protio-solvent resonances, and coupling constants are given in Hertz. Mass spectra were obtained by electrospray ionisation (positive and negative ionisation modes) on a Waters TQD mass spectrometer interfaced with an Acquity UPLC system with acetonitrile as the carrier solvent. Measurements requiring the use of an atmospheric solids analysis probe (ASAP) for ionisation were performed on Waters Xevo QToF mass spectrometer.

X-ray crystallography

The X-ray single crystal data for all compounds have been collected using λMoKα radiation (λ = 0.71073Å) at the temperature 120.0(2) K maintained by Cryostream (Oxford Cryosystems) open-flow nitrogen cryostats. The data for PtL^{1}Cl were collected on an Agilent XCalibur 4-circle κ-diffractometer (fine-focus tube, graphite monochromator, Sapphire CCD detector) and for compound PtL^{6}Cl - on a Bruker SMART 6K (fine-focus tube, graphite monochromator, SMART 6000 CCD detector) diffractometer. For all remaining compounds the data were collected on a Bruker D8Venture (Photon100 CMOS detector, IμS-microsource, focusing mirrors) 3-circle diffractometer. All structures were solved by direct methods and refined by full-matrix least squares on F^2 for all data using Olex2[46] and SHELXTL[47] software. All non-disordered non-hydrogen atoms were refined anisotropically, hydrogen atoms were placed into calculated positions and refined in riding mode. Crystal data and parameters of refinement are listed in Table S1 Crystallographic data for the structures have been deposited with the Cambridge Crystallographic Data Centre as supplementary publications CCDC 1943273–1943281.

Solution-state photophysics

UV-visible absorption spectra were recorded on a Biotek Instruments UVIKON XS spectrometer operating with LabPower software. Emission spectra were acquired on a Jobin Yvon Fluoromax-2 spectrometer equipped with a Hamamatsu R928 photomultiplier tube. All samples were contained

within 1 cm pathlength quartz cuvettes modified for connection to a vacuum line. Degassing was achieved by at least three freeze-pump-thaw cycles whilst connected to the vacuum manifold: final vapour pressure at 77 K was < 5 × 10^{-2} mbar. Emission was recorded at 90° to the excitation source, and spectra were corrected after acquisition for dark count and for the spectral response of the detector. The quantum yields were determined relative to an aqueous solution of $[Ru(bpy)_3]Cl_3$, for which $\Phi_{lum} = 0.028$.[48] Emission spectra at 77 K were recorded in 4 mm diameter tubes held within a liquid-nitrogen-cooled quartz dewar, uisng the same spectrometer.

The luminescence lifetimes in solution at 295 K were measured by time-correlated single-photon counting, using an EPL405 pulsed-diode laser as excitation source (405 nm excitation, pulse length of 60 ps, repetition rate 20 kHz). The emission was detected at 90° to the excitation source, after passage through a monochromator, using an R928 PMT thermoelectrically cooled to –20°C. The luminescence lifetimes at 77 K were recorded using the same detector operating in multichannel scaling mode, following excitation with a pulsed xenon lamp.

Synthetic and characterisation details for representative proligands and complexes

One example of each "class" of complex (as subdivided in Schemes 1 – 3) is given here, together with the corresponding proligand where isolated. Details for all other compounds prepared are given in the Supporting Information.

PtL^1Cl

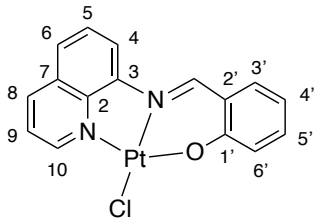

8-Aminoquinoline (0.10 g, 0.69 mmol) and salicylaldehyde (85 mg, 0.70 mmol) were placed under vacuum and heated to 65°C with stirring for 6 h. The crude proligand obtained, HL^1, is susceptible to hydrolysis (a process that is inhibited upon complexation), and was therefore used directly for complexation, without purification. A mixture of HL^1 (50 mg, 0.20 mmol), $Pt(COD)Cl_2$ (75 mg, 0.20 mmol), anhydrous triethylamine (20 mg, 0.20 mmol) and anhydrous acetonitrile (1 mL) was stirred overnight at reflux under argon. Upon cooling to ambient temperature, the precipitate that formed was separated by filtration and washed with successive portions of cold acetonitrile to give the title compound as a red solid (78 mg, 23% over two steps). ^{1}H NMR (DMSO-d_6, 600 MHz): 9.80 (1H, s, H^{imine}), 9.62 (1H, dd, J = 5.5 and 1, H^9), 8.86 (1H, d, J = 8, H^8), 8.78 (1H, d, J = 8, H^4),

8.06 (1H, d, J = 8, H^6), 7.92 (1H, t, J = 8, H^5), 7.85 – 7.83 (2H, m, H^{10} and $H^{3'}$), 7.56 (1H, ddd, J = 9, 6 and 2, $H^{5'}$), 6.97 (1H, d, J = 9, $H^{6'}$), 6.76 (1H, t, J = 7, $H^{4'}$). ^{13}C NMR (DMSO-d_6, 151 MHz): 163.7 ($C^{1'}$), 152.6 (C^9), 149.9 (C^{imine}), 146.7 (C^2), 144.2 (C^3), 139.8 (C^8), 135.9 ($C^{5'}$), 135.7 (C^{10} or $C^{3'}$), 129.6 (C^7), 129.2 (C^5), 128.3 (C^6), 124.2 (C^{10} or $C^{3'}$), 122.1 ($C^{2'}$), 121.8 ($C^{6'}$), 119.6 (C^4), 117.4 ($C^{4'}$). MS (ASAP): *m/z* 478 $[M+H]^+$; HRMS (ES+): *m/z* 476.0185 $[M]^+$; calculated for $[C_{16}H_{11}N_2OClPt]^+$ 476.0194.

PtL^2Cl, PtL^3Cl and PtL^4Cl were prepared similarly from 2-hydroxy-5-methoxybenzaldehyde, 2-hydroxy-5-(trifluoromethoxy)benzaldehyde, and 2-hydroxy-5-fluorobenzaldehyde, respectively, in place of salicylaldehyde (see Supporting Information).

HL^6

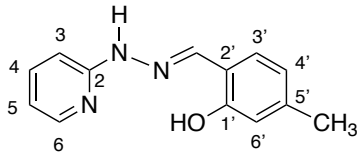

2-Hydroxy-4-methylbenzaldehyde (125 mg, 0.92 mmol) was added slowly to a stirred solution of 2-hydrazinopyridine (100 mg, 0.92 mmol) in MeOH (8 mL). The resulting white suspension was heated to reflux and stirred for 1 h. Upon cooling to room temperature, the precipitate that formed was removed by filtration and washed with hexane (2 × 2 mL) to give the title compound as a colourless solid (128 mg, 61%). ^{1}H NMR (DMSO-d_6, 600 MHz): 10.82 (1H, s, H^{NH}), 10.51 (1H, s, H^{OH}), 8.23 (1H, s, H^{imine}), 8.11 (1H, ddd, J = 5, 2, 1, H^3), 7.63 (1H, ddd, J = 9, 7, 2, H^5), 7.42 (1H, d, J = 8, $H^{3'}$), 6.99 (1H, d, J = 8.5, H^6), 6.75 (1H, ddd, J = 7, 5, 1, H^4), 6.71 (1H. s. $H^{6'}$), 6.69 (1H, d, J = 8, $H^{4'}$), 2.25 (3H, s, H^{Me}). ^{13}C NMR (DMSO-d_6, 151 MHz): 156.3 (C^2), 156.0 ($C^{1'}$), 148.0 (C^3), 139.1 ($C^{5'}$), 139.4 (C^{imine}), 138.0 (C^5), 127.4 ($C^{3'}$), 120.4 ($C^{4'}$), 117.7 ($C^{2'}$), 116.4 ($C^{6'}$), 114.9 (C^4), 106.0 (C^6), 21.1 (C^{Me}). MS (ES^-): *m/z* 226 $[M-H]^-$.

PtL^6Cl

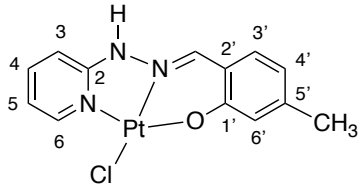

A solution of K_2PtCl_4 (50 mg, 0.12 mmol) in deionised water (1 mL) was added to a solution of HL^6 (25 mg, 0.12 mmol) in EtOH (2.5 mL) and the resulting pale pink solution was heated at reflux for 4 h with stirring. The resulting orange-brown precipitate was separated by centrifuge and washed successively with water (2 × 5 mL), EtOH (2 × 5 mL) and Et_2O (5 mL) to give the title

compound as a green solid (32 mg, 58%). ^{1}H NMR (DMSO-d_6, 700 MHz): 8.83 (1H, ddd, J = 6, 2, and 1, H^3), 8.61 (1H, s, H^{imine}), 7.95 (1H, ddd, J = 9, 7 and 2, H^5), 7.57 (1H, d, J = 8, $H^{3'}$), 7.20 (1H, ddd, J = 9, 2 and 1, H^6), 6.99 (1H, ddd, J = 7, 6 and 1, H^4), 6.91 (1H, s, $H^{6'}$), 6.61 (1H, dd, J = 8 and 2, $H^{4'}$), 2.19 (3H, s, H^{Me}). ^{13}C NMR (DMSO-d_6, 176 MHz): 159.6 ($C^{1'}$), 153.8 (C^2), 145.2 (C^3), 142.7 ($C^{2'}$), 138.3 (C^5), 138.1 (C^{imine}), 132.6 ($C^{3'}$), 120.5 ($C^{6'}$), 118.0 ($C^{4'}$), 116.3 ($C^{5'}$), 115.1 (C^4), 106.9 (C^6). MS (ES^-): *m/z* 456 $[M–H]^-$. HRMS (ES^+) *m/z* 456.0376 $[M+H]^+$, calculated for $[C_{13}H_{13}N_3OCl^{194}Pt]^+$ 456.0374.

HL[13]

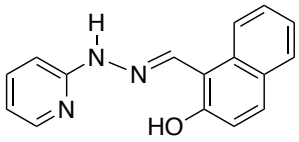

This compound was prepared using a procedure similar to that described in an earlier report, but where characterisation was limited to elemental analysis and an IR spectrum.[49] 2-Hydroxy-1-naphthaldehyde (230 mg, 1.34 mmol) was added to a solution of 2-hydrazinopyridine (146 mg, 1.34 mmol) in MeOH (5 mL). The resulting bright yellow slurry was heated at reflux with stirring for 30 min. Upon cooling to room temperature, the precipitate that formed was separated by filtration and washed with hexane (2 × 5 mL) to give the title compound as a bright yellow solid (301 mg, 85%). ^{1}H NMR ($CDCl_3$, 400 MHz): 11.89 (1H, br s), 8.85 (1H, s), 8.22 (1H, ddd, J = 5, 2 and 1), 8.01 (1H, d, J = 8), 7.79 (2H, t, J = 7.5), 7.69 (1H, ddd, J = 8, 7 and 2), 7.53 (1H, ddd, J = 8, 7 and 1), 7.38 (1H, ddd, J = 7.5, 7 and 1), 7.24 (2H, d, J = 9), 7.14 (1H, d, J = 8.5), 6.87 (1H, ddd, J = 7, 5 and 1). MS (ES+): *m/z* 264 $[M+H]^+$.

PtL[13]Cl

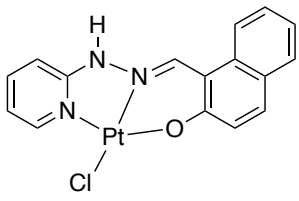

A solution of K_2PtCl_4 (50 mg, 0.12 mmol) in deionised water (1 mL) was added to a solution of HL^{13} (29 mg, 0.12 mmol) in EtOH (2.5 mL) and the resulting pale pink solution was heated at reflux with stirring for 4 h. The resulting green slurry was separated by centrifuge and the precipitate washed with water (2 × 5 mL), EtOH (2 × 5 mL) and Et_2O (5 mL) to give the title compound as a green solid (37 mg, 68%). ^{1}H NMR (DMSO-d_6, 400 MHz): 9.65 (1H, s), 8.86 (1H, d, J = 6), 8.08 (1H, d, J = 8.5), 7.99 (1H, ddd, J = 8.5, 7 and 1.5), 7.93 (1H, d, J = 9), 7.89 (1H, d, J

= 8), 7.65 (1H, t, J = 8), 7.38 (1H, t, J = 8), 7.33 – 7.30 (2H, m), 7.02 (1H, t, J = 7). MS (ES^-): *m/z* 492 $[M–H]^-$. HRMS (ES^+) *m/z* 492.0329, calculated for $[C_{16}H_{12}N_3OCl^{194}Pt]^+$ 492.0374.

HL^{14}

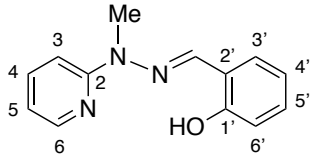

Salicylaldehyde (1.77 g, 14.5 mmol) was added to a solution of 2-(1-methylhydrazinyl)pyridine[50] (1.78 g, 14.5 mmol) in MeOH (20 mL). The resulting bright yellow solution was heated at reflux with stirring for 1 h. After cooling to room temperature, the solution was concentrated under reduced pressure until a precipitate began to form, and the mixture then placed in an ice bath for 30 min leading to further precipiation. The precipitate was separated by filtration and washed with hexane (2 × 10 mL) to yield the title compound as a cream solid (2.63 g, 80%). ^{1}H NMR (DMSO-d_6, 600 MHz): 10.38 (1H, s, H^{OH}), 8.23 (1H, d, J = 5, H^3), 8.05 (1H, s, H^{imine}), 7.71 (2H, t, J = 8, $H^{3'}$ and H^5), 7.47 (1H, d, J = 9, H^6), 7.19 (1H, t, J = 8, $H^{5'}$), 6.85-6.92 (3H, m, H^4, $H^{4'}$ and $H^{6'}$), 3.61 (3H, s, H^{NMe}). ^{13}C NMR (DMSO-d_6, 151 MHz): 156.8 (C^2), 155.7 (C^{OH}), 147.2 (C^3), 138.1 (C^5), 134.1 (C^{imine}), 129.5 ($C^{5'}$), 127.0 ($C^{3'}$), 121.2 ($C^{2'}$), 119.4 ($C^{6'}$), 116.0 ($C^{4'}$), 115.6 (C^4), 108.5 (C^6), 29.3 (C^{Me}). MS (ES^+): *m/z* 228 $[M+H]^+$, 108 $[M – C_7H_6NO+H]^+$; HRMS (ES^+): *m/z* = 228.1130 $[M+H]^+$; calculated for $[C_{12}H_{14}N_3O]^+$ 228.1137.

$PtL^{14}Cl$

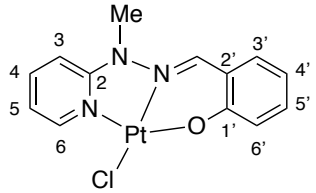

A solution of K_2PtCl_4 (50 mg, 0.12 mmol) in deionised water (1 mL) was added to a solution of HL^{14} (27 mg, 0.12 mmol) in EtOH (2.5 mL) and the resulting pale pink solution was heated at reflux with stirring for 4 h. The resulting mustard yellow precipitate was separated by centrifuge and washed successively with water (2 × 5 mL), EtOH (2 × 5 mL) and Et_2O (5 mL) to give a green solid. The crude product was then extracted into DCM and the resulting suspension was filtered through celite. The solvent was removed from the filtrate under reduced pressure to give the title compound as a yellow solid (45 mg, 82%). ^{1}H NMR (DMSO-d_6, 700 MHz): 9.06 (1H, ddd, J = 6, 2 and 0.5, H^3), 8.94 (1H, s, H^{imine}), 8.07 (1H, ddd, J = 9, 7 and 2, H^5), 7.82 (1H, dd, J = 8 and 2, $H^{3'}$), 7.48 (1H, d, J = 9, H^6), 7.45 (1H, ddd, J = 8.5, 6.5 and 2, $H^{6'}$), 7.09 (2H, m, H^4 and $H^{5'}$), 6.79 (1H, ddd, J = 8, 7 and 1, $H^{4'}$), 3.91 (3H, s, H^{NMe}). ^{13}C NMR (DMSO-d_6, 176 MHz): 159.3 (C^2), 152.9

($C^{1'}$), 145.9 (C^{3}), 138.7 (C^{5}), 137.6 (C^{imine}), 133.7 ($C^{3'}$), 132.5 ($C^{5'}$), 120.5 ($C^{6'}$), 118.8 ($C^{2'}$), 116.1 ($C^{4'}$), 115.8 ($C^{4'}$), 108.7 (C^{6}), 34.03 (C^{NMe}). MS (ES+): *m/z* 462 $[M–Cl+MeCN]^+$; HRMS (ES+): *m/z* 461.0865 $[M+H]^+$; calculated for $[C_{15}H_{15}N_4OPt]^+$ 461.0878.

HL[18]

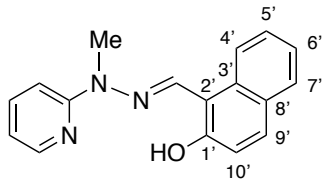

2-Hydroxy-1-napthaldehyde (105 mg, 0.61 mmol) was added to a stirring solution of 2-(1-methylhydrazinyl)pyridine (75 mg, 0.61 mmol) in MeOH (3 mL). The resulting lemon-coloured slurry was heated at reflux with stirring for 30 min. Upon cooling to room temperature, the precipitate that had formed was separated by filtration and washed with cold MeOH (2 × 5 mL) to give the title compound as cream solid (148 mg, 87%). ^{1}H NMR ($CDCl_3$, 700 MHz): 12.43 (1H, s, H^{OH}), 8.67 (1H, s, H^{imine}), 8.30 (1H, ddd, J = 5, 2 and 1, H^{3}), 8.11 (1H, d, J = 8.5, $H^{4'}$), 7.81 (1H, d, J = 8, $H^{7'}$), 7.76 (1H, d, J = 9, $H^{9'}$), 7.67 (1H, ddd, J = 8.5, 7 and 2, H^{5}), 7.54 (1H, ddd, J = 8.5, 7 and 1, $H^{6'}$), 7.38 (1H, ddd, J = 8, 7 and 1, $H^{5'}$), 7.35 (1H, d, J = 8.5, H^{6}), 7.25 (1H, d, J = 8, $H^{10'}$), 6.86 (1H, dd, J = 7, 5 and 1, H^{4}), 3.83 (3H, s, H^{NMe}). ^{13}C NMR ($CDCl_3$, 176 MHz): 156.6 (C^{2}), 156.5 ($C^{1'}$), 147.6 (C^{3}), 138.4 (C^{5}), 134.9 (C^{imine}), 132.0 ($C^{8'}$), 131.2 ($C^{9'}$), 129.3 ($C^{7'}$), 128.6 ($C^{3'}$), 127.2 ($C^{6'}$), 123.4 ($C^{5'}$), 120.2 ($C^{4'}$), 119.1 ($C^{10'}$), 116.3 (C^{4}), 109.8 ($C^{2'}$), 108.6 (C^{6}). MS ($ES^–$): *m/z* 276 $[M–H]^–$.

PtL[18]Cl

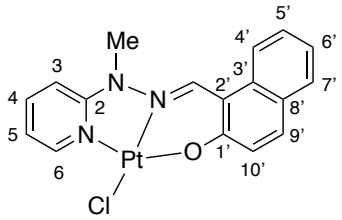

A solution of K_2PtCl_4 (75 mg, 0.18 mmol) in deionised water (1.5 mL) was added to a solution of HL^{18} (50 mg, 0.17 mmol) in EtOH (4 mL) and the resulting pale pink solution was heated at reflux with stirring for 4 h. The resulting green precipitate was separated by centrifuge and washed successively with water (2 × 5 mL), EtOH (2 × 5 mL) and Et_2O (5 mL). The crude green product was recrystallized from hot DMF to give the title compound as a yellow solid (30 mg, 35%). ^{1}H NMR (DMSO-d_6, 700 MHz): 9.45 (1H, s), 9.06 (1H, d, J = 7), 8.41 (1H, d, J = 8.5), 8.08 (1H, t, J = 8), 7.92 (1H, d, J = 9), 7.85 (1H, d, J = 8), 7.61 (1H, t, J = 7.5), 7.56 (1H, d, J = 9), 7.36 (1H, t, J = 7), 7.30 (1H, d, J = 9), 7.10 (1H, t, J = 6). The material was not sufficiently soluble to obtain a ^{13}C

NMR spectrum. MS (ES+): *m/z* 507 $[M+H]^+$. HRMS (ES^+) *m/z* 507.0626, calculated for $[C_{17}H_{14}N_3OCl^{194}Pt]^+$ 507.0614.

PtL^1-C≡C-Ar

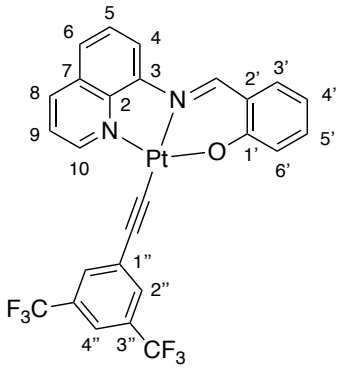

A mixture of PtL^{1}Cl (30 mg, 0.06 mmol), CuI (5 mg, 0.03 mmol), 1-ethynyl-3,5-bis(trifluoromethyl)benzene (23 mg, 0.10 mmol) and anhydrous NEt_3 (0.3 mL) in anhydrous DCM (3 mL) was heated at reflux for 48 h under argon. The solvent was removed under reduced pressure and the resulting crude material purified by column chromatography (hexane / DCM, gradient elution 80:20 to 20:80) to yield the title compound as a red solid (21 mg, 50%). ^{1}H NMR (DMSO-d_6, 700 MHz): 9.80 (1H, d, J = 5, H^{10}), 9.15 (1H, s, H^{imine}), 8.49 (1H, d, J = 8, H^8), 8.23 (1H, d, J = 7.5, H^4), 7.96 (2H, s, $H^{2''}$), 7.79 (1H, d, J = 8, H^6), 7.74 (1H, t, J = 8, H^5), 7.70 (1H, s, $H^{4'}$), 7.52-7.47 (3H, m, H^9, $H^{3'}$ and $H^{5'}$), 7.06 (1H, d, J = 9, $H^{6'}$), 6.67 (1H, t, J = 7, $H^{4'}$). ^{13}C NMR (DMSO-d_6, 176 MHz): 165.5 (C^3), 154.9 (C^{10}), 149.7 (C^{imine}), 146.4 ($C^{1'}$), 145.3 (C^2), 138.7 (C^5), 136.0 ($C^{3'}$ or $C^{5'}$), 135.4 ($C^{3'}$ or $C^{5'}$), 132.4 ($C^{2''}$), 131.5 (C^{CF_3}), 130.2 (C^8), 129.0 (C^5), 127.6 (C^6), 124.8 ($C^{1'''}$), 123.9 (C^9), 123.2 ($C^{6'}$ and $C^{2'''}$), 119.1 ($C^{4''}$), 117.7 (C^2), 117.5 ($C^{4'}$), 101.3 ($C^{2'}$), 96.5 ($C^{1''}$). MS (ES+): *m/z* 679 $[M+H]^+$; HRMS (ES+): *m/z* 679.0731 $[M+H]^+$; calculated for $[C_{26}H_{15}N_2OF_6Pt]^+$ 679.0715.

Crystallisation of complexes

Single crystals of PtL^{1}Cl and PtL^1(C≡C-Ar) suitable for X-ray diffraction analysis were obtained by slow evaporation of a solution in DCM or the cooling of a concentrated solution in DMSO, respectively. Crystals of the former contain one molecule of CH_2Cl_2 per molecule of PtL^{1}Cl, whilst the latter contains two molecules of Me_2SO. Amongst the hydrazone complexes containing N–H functionality, crystals of PtL^{6}Cl, PtL^{8}Cl, and PtL^{12}Cl were obtained by recrystallisation from DMF, DMSO, and DMF respectively. The crystal of PtL^{6}Cl contains one molecule of DMF per molecule of complex, that of PtL^{8}Cl one molecule of DMSO, and that of PtL^{12}Cl one molecule of H_2O. In PtL^{12}Cl, the water molecules in the lattice participate in H-bonding with the N–H of the hydrazone. For the N-methylhydrazone class of complexes, suitable crystals were obtained of PtL^{14}Cl, PtL^{17}Cl and PtL^{19}Cl from DMF solutions, of which PtL^{17}Cl has one molecule of DMF per complex; crystals

of $PtL^{20}Cl$ were obtained from DMSO and they incorporate one DMSO molecule per complex. Table S1 in the Supporting Information provides crystal data and structure refinement parameters.

Conflicts of Interest

There are no conflicts of interests to declare.

Acknowledgements

We thank EPSRC and Durham University for support.

Supporting Information

Electronic supporting information is available: additional figures showing molecular structures and crystal packing in the crystals; frontier orbital plots obtained by DFT; additional absorption and emission spectra; synthesis and characterisation of all other materials not already included in the Eperimental Section above.

References

1. (a) D. R. McMillin, J. J. Moore, *Coord. Chem. Rev.,* 2002, **229**, 113; (b) J. A. G. Williams, *Top. Curr. Chem.,* 2007, **281**, 205; (c) R. McGuire, M. C. McGuire, D. R. McMillin, *Coord. Chem. Rev.,* 2010, **254**, 2574; (d) L. Murphy, J. A. G. Williams, *Top. Organomet. Chem.,* 2010, **28**, 75; (e) Y. Chi, P. T. Chou, *Chem. Soc. Rev.,* 2010, **39**, 638; (f) A. Diez, E. Lalinde and M. T. Moreno, *Coord. Chem. Rev.*, 2011, **255**, 2426; (g) K. Li, G. S. M. Tong, Q. Y. Wan, G. Cheng, W. Y. Tong, W. H. Ang, W. L. Kwong, C.M. Che, *Chem. Sci.,* 2016, **7**, 1653.
2. (a) W.Y. Wong and C.L. Ho, *Chem. Soc. Rev.,* 2009, **253**, 1709; (b) J. Kalinowski, V. Fattori, M. Cocchi, J.A.G. Williams, *Coord. Chem. Rev.,* 2011, **255**, 2401; (c) C.M. Che, C.C. Kwok, S.W. Lai, A.F. Rausch, W. J. Finkenzeller, N. Y. Zhu, H. Yersin, *Chem. Eur. J.,* 2010, **16**, 233; (d) S. Q. Huo, J. Carroll and D. A. K. Vezzu, *Asian J. Org. Chem.,* 2015, **4**, 1210.
3. (a) P. Wu, E. L. M. Wong, D. L. Ma, G. S. M. Tong, K. M. Ng and C. M. Che, *Chem. Eur. J.*, 2009, **15**, 3652; (b) W. L. Tong, M. C. W. Chan and S. M. Yiu, *Organometallics,* 2010, **29**, 6377; (c) Q. Zhao, C. Huang and F. Li, *Chem. Soc. Rev.,* 2011, **40**, 2508; (d) K. K. W. Lo, A. W. T. Choi and W. H. T Law, *Dalton Trans.,* 2012, **41**, 6021; (e) Z. Guo, W. L. Tong and M. C. W. Chan, *Chem. Commun.,* 2014, **50**, 1711; (f) M. Mauro, A. Aliprandi, D. Septiadi, N. S. Kehra and L. De Cola, *Chem. Soc. Rev.,* 2014, **43**, 4144; (g) E. Lalinde, R. Lara, I. P. Lopez,

M. T. Moreno, E. Alfara-Arnedo, J. G. Pichel and S. Pineiro-Hermida, *Chem. Eur. J.,* 2018, **24**, 2440.

4. (a) E. Baggaley, J. A. Weinstein and J. A. G. Williams, *Coord. Chem. Rev.* 2012, **256**, 1762; (b) E. Baggaley, J. A. Weinstein and J. A. G. Williams, *Struct. Bond.* 2015, **165**, 205.
5. G. Liebsch, I. Klimant, B. Field, G. Holst, O. S. Wolfbeis, *Appl. Spectrosc.*, 2000, **54**, 548.
6. (a) J. Z. Zhao, W. H. Wu, J. F. Sun, S. Guo, *Chem. Soc. Rev.,* 2013, **42**, 5323; (b) F. N. Castellano, *Acc. Chem. Res.,* 2015, **48**, 828.
7. (a) R. E. Doherty, I. V. Sazanovich, L. K. McKenzie, A. S. Stasheuski, R. Coyle, E. Baggaley, S. Bottomley, J. A. Weinstein and H. E. Bryant, *Sci. Rep.*, 2016, **6**, 22668; (b) L. K. McKenzie, H. E. Bryant and J. A. Weinstein, *Coord. Chem. Rev.,* 2019, **379**, 2; *(c)* A. Colombo, M. Fontani, C. Dragonetti, D. Roberto, J. A. G. Williams, R. Scotto di Perrotolo, F. Casagrande, S. Barozzi and S. Polo, *Chem. Eur. J.*, 2019, **25**, 7948.
8. H. Yersin, A. F. Rausch, R. Czerwieniec, T. Hofbeck, T. Fischer, *Coord. Chem. Rev.,* 2011, **255**, 2622.
9. A. Rausch, L. Murphy, J. A. G. Williams, H. Yersin, *Inorg. Chem.,* 2012, **51**, 312.
10. (a) C. J. Ballhausen, N. Bjerrum, R. Dingle, K. Eriks, C. R. Hare, *Inorg. Chem.,* 1965, **4**, 514; (b) V. Balzani, V. Carassiti, *J. Phys. Chem.,* 1968, **72**, 383.
11. L. J. Andrews, *J. Phys. Chem.* 1979, **83**, 3203.
12. G. T. Morgan and F. H. Burstall, *J. Chem. Soc.,* 1934, 1498.
13. K. L. Garner, L. F. Parkes, J. D. Piper and J. A. G. Williams, *Inorg. Chem.,* 2010, **49**, 476.
14. (a) S. J. Farley, D. L. Rochester, A. L. Thompson, J. A. K. Howard and J. A. G. Williams, *Inorg. Chem.*, 1005, **44**, 9690. (b) J. A. G. Williams, *Chem. Soc. Rev.* 2009, **38**, 1783.
15. (a) E. C. Constable, R. P. G. Henney, T. A. Leese and D. A. Tocher, *J. Chem. Soc., Dalton Trans.,* 1990, 443. (b) S. W. Lai, M. C. W. Chan, T. C. Cheung, S. M. Peng, C. M. Che, *Inorg. Chem.* 1999, **38**, 4046.
16. G. S. M. Tong, C. M. Che, *Chem. Eur. J.* 2009, **15**, 7225.
17. (a) L. P. Ardasheva, G. A. Shagisultanova, *Russ. J. Inorg. Chem.,* 1998, **43**, 85; (b) C. M. Che, S. C. Chan, H. F. Xiang, M. C. W. Chan, Y. Liu, Y. Wang, *Chem. Commun.,* 2004, 1484.
18. Y. Y. Lin, S. C. Chan, M.C.W. Chan, Y. J. Hou, N. Zhu, C.M. Che, Y. Liu, Y. Wang, *Chem. Eur. J.,* 2003, **9**, 1264.
19. C. C. Kwok, H. M. Y. Ngai, S. C. Chan, I. H. T. Sham, C. M. Che, N. Zhu, *Inorg. Chem.,* 2005, **44**, 4442.
20. D. A. Bardwell. J. G. Crossley, J. C. Jeffery, A. G. Orpen, E. Psillakis, E. E. M. Tilley and M. D. Ward, *Polyhedron*, 1994, **13**, 2291.

21. B. M. Dahl, O. Dahl, *Acta Chem. Scand.,* 1969, **23**, 1503.
22. A. Sarkar and S. Pal, *Polyhedron*, 2006, **25**, 1689.
23. D. Ramakrishna and B. R. Bhat, *Inorg. Chem. Commun.*, 2010, **13**, 195.
24. W. Cao, Y. Liu, T. Zhang and J. Jia, *Polyhedron*, 2018, **147**, 62.
25. (a) V. W. W. Yam, R. P. L. Tang, K. M. C. Wong and K. K. Cheung, *Organometallics*, 2001, **20**, 4476; (b) Q. Z. Yang, L. Z. Wu, Z. X. Wu, L. P. Zhang and C. H. Tung, *Inorg. Chem.,* 2002, **41**, 5653; (c) V. W. W. Yam, K. M. C. Wong and N. Zhu, *J. Am. Chem. Soc.,* 2002, **124**, 6506.
26. X. Zhou, H. X. Zhang, Q. J. Pan, B. H. Xia and A. Tang, *J. Phys. Chem. A,* 2005, **109**, 8809.
27. W. Lu, B. X. Mi, M. C. W. Chan, Z. Hui, C. M. Che, N. Zhu and S. T. Lee, *J. Am. Chem. Soc.,* 2004, **126**, 4958.
28. (a) H. J. Keller (ed), *Chemistry and Physics of One-Dimensional Metals*, Plenum Press, New York, 1977. (b) J. S. Miller (ed), Extended Linear Chain Compounds, Plenum Press, New York, 1982.
29. H. K. Yip, L. K. Cheng, K.K. Cheung and C. M. Che, *J. Chem. Soc. Dalton Trans.* 1993, 2933.
30. V. W. W. Yam, R. P. L. Tang, K. M. C. Wong and K. K. Cheung, *Organometallics*, 2001, **20**, 4476.
31. G. Asgedom, A. Sreedhara, J. Kivikoski, E. Kolehmainen and C. P. Rao, *J. Chem. Soc., Dalton Trans.* 1996, 93.
32. J. W. Ledbetter, *J. Phys. Chem.* 1966, **70**, 2245.
33. K. Huang and A. Rhys, *Proc. Roy. Soc.* 1950, **204**, 406.
34. A. Juris, V. Balzani, F. Barigelletti, P. Belser and A. von Zelewsky, *Coord. Chem. Rev.,* 1988, **84**, 85.
35. T. Sajoto, P. I. Djurovich, A. B. Tamayo, J. Oxgaard, W. A. Goddard and M. E. Thompson, *J. Am. Chem. Soc.,* 2009, **131**, 9812.
36. (a) R. Englman and J. Jortner, *Mol. Phys.,* 1970, **18**, 145. (b) J. V. Caspar, E. M. Kober, B. P. Sullivan and T. J. Meyer, *J. Am. Chem. Soc.,* 1982, **104**, 630.
37. D. N. Kozhevnikov, V. N. Kozhevnikov, M. Z. Shafikov, A. M. Prokhorov, D. W. Bruce and J. A. G. Williams, *Inorg. Chem.,* 2011, **50**, 3804.
38. F. N. Castellano, I. E. Pomestchenko, E. Shikhova, F. Hua, M. L. Muro and N. Rajapakse, *Coord. Chem. Rev.,* 2006, **250**, 1819.
39. E. Rossi, A. Colombo, C. Dragonetti, D. Roberto, R. Ugo, A. Valore, L. Falciola, P. Brulatti, M. Cocchi and J. A. G. Williams, *J. Mater. Chem.,* 2012, **22**, 10650.

40. M. Chang, H. Horiki, K. Nakajima, A. Kobayashi, H.-C. Chang and M. Kato, *Bull. Chem. Soc. Jpn.*, 2010, **83**, 905.
41. M. Chang, A. Kobayashi, H.-C. Chang, K. Nakajima and M. Kato, *Chem. Lett. Jpn.*, 2011, **40**, 1335.
42. A. Bacchi, M. Carcelli, M. Costa, A. Fochi, C. Monici, P. Pelagetti, C. Pelizzi, G. Pelizzi and L. M. S. Roca, *J. Organomet. Chem.,* 2000, **593-594**, 180.
43. M. Mohan, N. S. Gupta, L. Chandra and N. K. Jha, *J. Inorg. Biochem.*, 1987, **31**, 7.
44. C. C. Hsu, C. C. Lin, P. T. Chou, C. H. Lai, C. W. Hsu, C. H. Lin and Y. Chi, *J. Am. Chem. Soc.,* 2012, **134**, 7715.
45. M. Mydlak, M. Mauro, F. Polo, M. Felicetti, J. Leonhardt, G. Diener, L. De Cola and C. A. Strasert, *Chem. Mater.,* 2011, **23**, 3659.
46. O. V. Dolomanov, L. J. Bourhis, R. J. Gildea, J. A. K. Howard and H. Puschmann, *J. Appl. Cryst.,* 2009, **42**, 339.
47. G. M. Sheldrick, *Acta Cryst.,* 2008, **A64**, 112.
48. K Nakamaru, *Bull. Chem. Soc. Jpn*, 1982, **55**, 2697.
49. S. Mukherjee, S. Chowdhury, A. Ghorai, U. Ghosh and H. Stoeckli-Evans, *Polyhedron*, 2013, **51**, 228.
50. D. Leung and E. V Anslyn, *Org. Lett.,* 2011, **13**, 2298.